SAPIENZA
Università di Roma
Facoltà di Scienze Matematiche Fisiche e Naturali

DOTTORATO DI RICERCA
IN BIOLOGIA CELLULARE E DELLO SVILUPPO

XXXII Ciclo
(A.A. 2019/2020)

The neurotoxicity of native metastable prefibrillar oligomers from salmon Calcitonin: an innovative amyloid-induced excitotoxicity paradigm.

Dottorando
Dr. Marcello Belfiore - Istituto Superiore di Sanità

Docente guida
Prof.ssa M.E. De Stefano, PhD

Tutori
Dr. Marco Diociaiuti & Dr. Claudio Frank.
Istituto Superiore di Sanità

Coordinatore
Prof.ssa Giulia De Lorenzo

Abstract

Protein misfolding is implicated in different severe amyloid-related neurodegenerative diseases, like Alzheimer's, Parkinson's and Creutzfeldt-Jacob's. This process results in the aggregation of toxic small soluble prefibrillar oligomers (PFOs), almost ineffective proto-fibrils (PFs) and mature fibres (MFs). Many efforts are pointing to clarify PFOs structures and cytotoxicity. However, since their metastability, oligomers change their conformation along with the experiments leading to inconsistency in comparing data from different groups. Salmon Calcitonin (sCT), is a 32 amino acid polypeptide hormone displaying the tendency to self-assemble in the amyloid pattern, with a very low aggregation rate. This appealing feature allows investigating the effects of native PFOs in the early stages of neurotoxicity, without any chemical stabilization. We purified sCT PFOs enriched fractions by means of size exclusion chromatography (SEC) aiming to find who is the most toxic species, among sCT PFOs, comparing the biologic effects of native PFOs enriched fraction respect to sCT monomers. The intracellular Ca^{2+} rise plays a fundamental role in amyloid protein-induced neurodegenerations. According to what we found in literature, two paradigms have been explored: i) the "membrane permeabilization" due to the formation of amyloid pores or other types of membrane damage; ii) "receptor-mediated" modulation of Ca^{2+} channels. Therefore, we tested the effects of native sCT PFOs or monomers in differentiated neurons, employing Ca^{2+}imaging, cellular viability, Long-Term Potentiation (LTP), post-synaptic densities protein expression, excised patch-clamp recordings, and miniature-Excitatory Post-Synaptic Currents (mEPSC). Results indicated that PFOs-, but not Monomer-enriched solutions, induced abnormal permeability to Ca^{2+}, not fully explained by N-methyl-D-aspartate receptors (NMDARs) activation. We also found that the formation of small amyloid pores was consistent with an increased quantal release of neurotransmitters, able to drive a receptor-mediated response, *per se*. Thus, we propose an innovative neurotoxicity mechanism for amyloid proteins where the "membrane permeabilization" and "receptor-mediated" paradigms coexist.

Introduction

Biological systems evolved elaborate mechanisms to ensure correct protein folding or otherwise detection/degradation of unfolded proteins, to prevent any cellular harm[1–3]. This is especially true considering the extent of the human proteome, estimated between 10000 and several billion of proteins[4].

The most intriguing ability of all living systems is to self-assemble complex macromolecules with precision and fidelity. The "native state" of proteins (fully folded proteins) corresponds to the most thermodynamically stable structures under physiological conditions. It has become clear that the folding is a stochastic process where native-prone interactions between residues, of the primary protein, are more stable than those not-native-prone, consequently, the polypeptide chain can auto-determine its most stable structure[3]. *In vitro,* during transitions from random coil structures to the native state, the residues interactions within the polypeptide main chain may be modelized using computational chemical-dynamics simulation, based on data obtained *in vitro* by X-ray diffraction and NMR-spectroscopy. The "energy landscape" of these interactions revealed that in physiological conditions only a small number of all conformations is possible by any given protein molecule. This is why proteins fold rapidly and efficiently[5,6].

In vivo, folding occurs while the new-born polypeptide chain is still attached to the ribosome, or in specific cellular compartments, such as mitochondria, or the endoplasmic reticulum (ER). Finally, native proteins are transferred towards their destination, by trafficking and translocation through membranes[7] (Fig.1). Since incompletely folded proteins inevitably expose to the solvent at least some regions of the structure, normally hidden in the native state, they are prone to inappropriate interaction with other molecules within the crowded environment of the cell. Living systems have been therefore evolved strategies to prevent such behaviour[7–9].

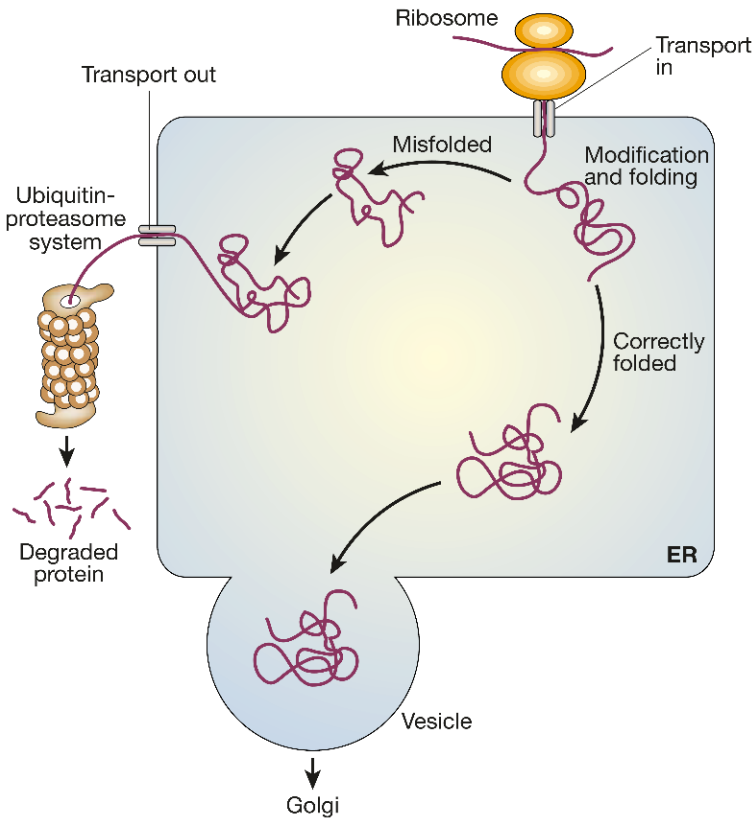

Figure 1- Protein folding mechanisms toward the native state – Taken from Dobson 2003

Molecular chaperons contain cavities where unfolded polypeptide domains undergo folding, toward their native structures protected from the outside world[3,10]. Moreover, the folding catalyst accelerates the slow steps of the process (like cis-trans isomerization and formation/reorganization of disulphide bonds)[11]. These proteins protect against competing reactions, particularly aggregation.
All these "quality-control" checks, enable correctly folded proteins to be distinguished from misfolded ones[12] that have to be degraded by the ubiquitin-proteasome system[13] (Fig.1).

Despite primary peptide sequences, the misfolding process often results in a self-assembling behaviour and thus in the aggregation

of small soluble oligomers sharing conformations and dimensions. In the early stages of this process, a dynamic range equilibrium is achieved between small unfolded- (Random coiled) and intermediate folded-aggregates (disordered) (Fig.2). These metastable structures are named as pre-fibrillar oligomers (PFOs). As the oligomerization moves forward, random coiled structures interchange into β-sheet conformation and Proto- and insoluble Mature- Fibres (PFs and MFs) appear. This happens after a lag phase, whose duration is depending on protein concentration, ionic strength, pH and temperature. Upon the formation of a critical β-sheet core, aggregation is auto-determined, and the fibre elongation proceeds fast.

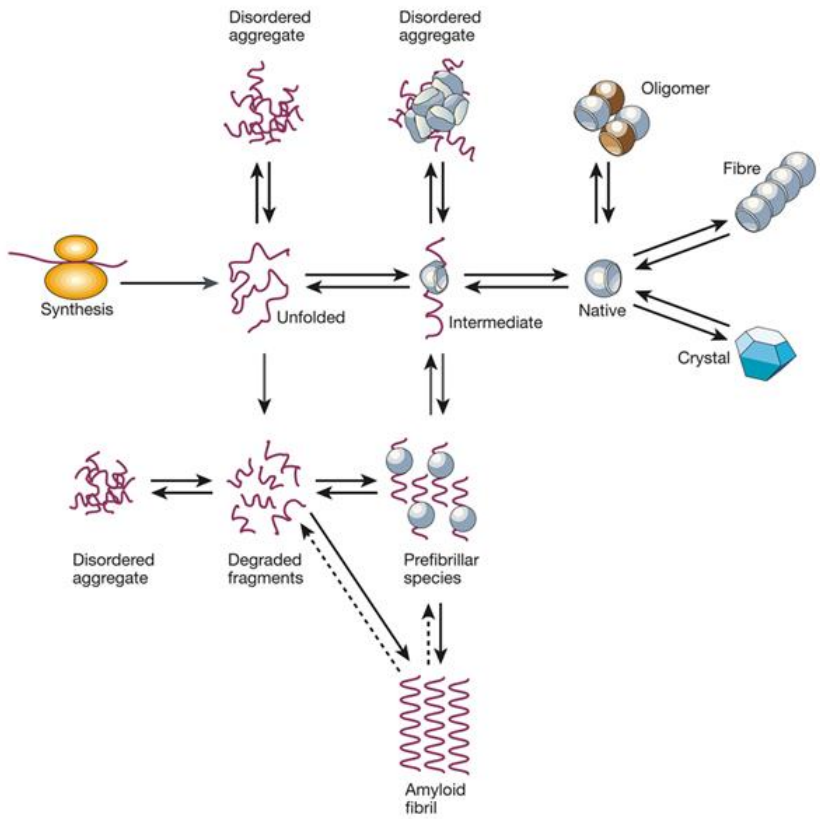

Figure 2 - the amyloid aggregation pathway– Taken from Dobson 2003

These aggregates have been defined as “amyloid” since they resemble some properties of the starch (amylose): the optical redshift in the light absorption of the Congo red dye, the characteristic green birefringence under polarized light and a characteristic “cross-β” structure in X-ray diffraction Electron microscopy. All these features are generally required to be properly described as amyloid[14].

A range of debilitating human diseases is associated with protein misfolding[14–16], including several neurodegenerative diseases like Alzheimer’s, Parkinson’s, the Creutzfeldt–Jakob spongiform encephalopathies and type II diabetes; each one is associated with plaques and aggregates of specific monomers [3,8,16] (Amyloid β, Tau, α-Synuclein, Prion’s Protein,.., Etc).

The ability of polypeptide chains to form amyloid structures seems to be a generic feature of every polypeptide fibrils can be formed *in vitro* by denaturing with heat or chemicals any known proteins or polypeptide: such as myoglobin and polylysine[14,17]. Under certain conditions the protein unfolds, at least partially, exposing specific six amino acids long elements[8]. These “amyloidogenic segments”, tightly interact with the same counterpart on another native protein[18], inducing a loop of protein’s misfolding, a process named seeding[8,19]. The nucleation event may be rare, but once it starts, it never ends[18]. This aggregating character it is supposed to be the default behaviour of each protein, in absence of any stabilization mechanism; a sort of “Dark Side of proteins”[8]

Calcitonin (CT), is a 32 amino acid polypeptide hormone, secreted in the ultimo-pharyngeal body of the fish[20] and the thyroid of mammals with a pivotal role in the blood calcium maintenance and bone homeostasis; It was also used in the past for the therapy of osteoporosis[21]. CT displays the tendency to self-assemble in the amyloid pattern[22,23]. Among CT variants, salmon Calcitonin (sCT), present the lowest aggregation rate[22]. Just to give insight, the human CT lag phase is 21 hours (1mg/mL, 22°C in 50mM Tris/HCl buffer, pH7.4), for the sCT in the same conditions is above 8 month[22].

This appealing feature allows us to investigate the effects of native sCT PFOs in the early stages of neurotoxicity, without any chemical stabilization procedure, including for "Photo-induced cross-linking of unmodified proteins[1]" (PICUP), as well as the possibility to get a new insight in the early mechanisms of neurodegeneration.

It is now accepted that the intracellular Ca^{2+} elevation represents a common mechanism in amyloid toxicity leading cells to death[24]. Up to now, two paradigms have been explored in the literature to explain the observed Ca^{2+}-influx upon PFOs administration and the following toxicity[25]:

i) the "membrane permeabilization" hypothesis, where the interactions between oligomers and lipid membranes expressing monosialoganglioside-GM1 [26–29] results in membrane leakage or the formation of pore-like structures, increasing permeability to electrolytes [30,31]. Shafrir and co-workers, based on transmission electron- and atomic force microscopy data, simulated in Molecular Dynamics the formation of stable amyloid pores[32].
Very recently Bode and colleagues demonstrated ion-channel formation induced by $A\beta_{1\text{-}42}$ oligomers but not by SEC-purified Monomers in a cellular patch of membranes excised from HEK-293 cell line[33].

ii) the "receptor-mediated" hypothesis, where amyloid oligomer modulation of Ca^{2+} permeable channels such as n-methyl-d-aspartate receptors (NMDARs) or voltage-dependent Ca^{2+} channels (VDCC), leads to an abnormal intracellular Ca^{2+} elevation[34]. Several groups stressed the relationship between Aβ oligomers and NMDARs mediated excitotoxicity[35,36]. Peters et al. demonstrated that Aβ-evoked currents in hippocampal neurons are proportional to neuronal NMDARs expression[36]. amyloid oligomers can elevate intracellular Ca^{2+}, through a signalling pathway depending upon specific Ca^{2+}/calmodulin protein phosphatases at postsynaptic

densities[34,37] (PSD). Other groups reported that, in hippocampal neurons, Aβ oligomers act on metabotropic glutamate receptors-5 (mGluR5), resulting in the activation of JNK, Cdk5 and p38 MAPK pathways[34,38–40]. Moreover, it has been also suggested that inhibition of the long term potentiation (LTP) would be a consequence of Aβ-oligomers interference with glutamate synaptic reuptake mechanism[41]. Notably, it is well known that the Ca^{2+} channel occurrence is correlated to the lipid-rafts and then to the GM1 expression.

Aim of the work

During my PhD project, we used sCT as a tool to investigate the early molecular mechanisms underlying amyloid neurotoxicity. According to literature, we aimed to clarify the receptors mediated- and pore mediated-effects and their relationship with GM1-lipid-rafts expression. Therefore, we planned the following experiments:

1. In neuronal lines/cultures, characterized by increasing degree of differentiation and thus in GM1 content (HT-22, HT-22 DIFF, HpC 6 DIV, HpC 14 DIV, where DIV stays for "day-*in vitro"*), we assessed the effects of native sCT PFOs- respect to Monomer-enriched solutions, in terms of intracellular Ca^{2+}-elevation, cellular viability, synaptic protein expression, LTP impairment,
2. We aimed to demonstrate the amyloid pore formation in excised patches of membrane from primary hippocampal neurons, measuring in inside-out patch-clamp recordings, the transmembrane currents elicited by native sCT PFOs- and Monomer-enriched solutions, at a single-channel resolution, as compared to those seen with known ionophores.
3. In voltage-clamp experiments, we evaluated the effects of sCT PFOs- and Monomers on the spontaneous quantal release of neurotransmitters, in primary neurons from the hippocampus, by recording spontaneous miniature excitatory postsynaptic currents (mEPSC).

Our results[42] strongly indicate that native metastable sCT PFOs induced neurotoxic effects whose amplitude correlates with the differentiation degree of neuronal cultures, while Monomers were always ineffective.

The same data disagree with the idea that oligomers directly have effects on receptors because also monomers should drive toxicity otherwise, even if at lower levels. On the other hand, sCT- and other amyloid-PFOs appear to behave in the same common way mediated by NMDARs, therefore we ask how it could be possible to drive receptors or channels so specifically through very different protein sequences,

this is not expected. Consequently, a common “amyloid mediated neurotoxicity mechanism” based on the interactions of these aggregates with lipid membranes, but independent on their specific sequence, might exists.

Moreover, we show that PFOs effects might be correlated to neuronal membrane permeabilization and possibly to an increased neurotransmitter quantal release.

Thus, we propose for the first time, a possible mechanism where both “membrane permeabilization” and “receptor-mediated” paradigms could contribute to explain the amyloid neurotoxicity. We speculate that in mature neurons PFOs, but not Monomers, may induce initial membrane permeabilization that triggers a subsequent abnormal quantal release and consequently an NMDARs-mediated Ca^{2+}-influx, leading to the observed LTP impairment and neurotoxicity.

Results

Sample preparation and characterization.

Native sCT solution was prepared by incubating 2 mg of lyophilized sCT in phosphate buffer (5 mM) at room temperature overnight. We previously demonstrated that, under these conditions, the formation of PFOs was facilitated in respect of MFs[43]. To purify oligomeric species enriched fractions, the aggregated and native solution was then loaded in the SEC column[43]. The SEC profile of sCT spontaneously aggregated mixture is presented in Fig. 3a. The absorbance profile, at 280 nm, of the SEC fractions, is characterized by a peak around 29th fraction (V_e=24.65 mL), followed by a prolonged tail. According to the calibration standards elution profile (Fig.3b), the peak (6450 Da) is near a dimer. The prolonged tail on the right is because Monomers (3400 Da) are uniformly distributed over fractions at a very low concentration. Consequently, we prepared Monomer-enriched sCT solution by dissolving the powder in desalted water just before treatments, at a concentration of 80 µM (like t
he 29th fraction concentration), since the aggregation dynamics depends upon ionic strength and concentration.

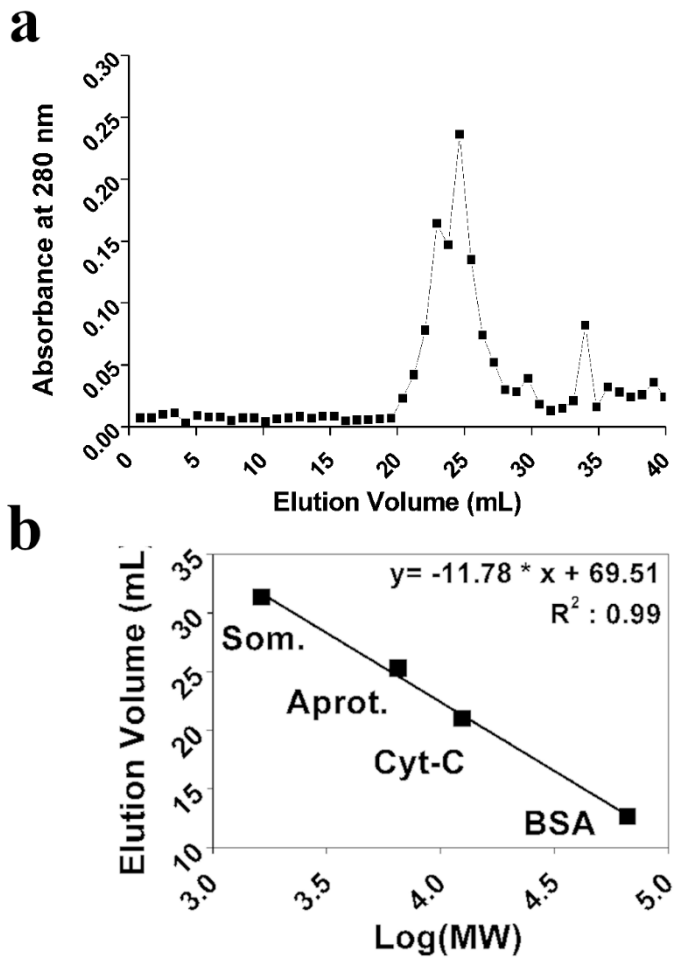

*Figure 3 – **(a)** The Size Exclusion Chromatography elution profile of the spontaneously aggregated sCT sample. The main peak, relative to PFOS, can be observed around 29th fraction corresponding to Ve=24.65 mL. **(b)** the calibration regression gives for the 29th fraction an MW=6450 Da, which is about an sCT dimer*[42].

The characterization of the collected fractions, from the SEC peak and native Monomers-enriched samples, has been obtained after the PICUP procedure followed by tricine SDS-PAGE (Fig. 4a).

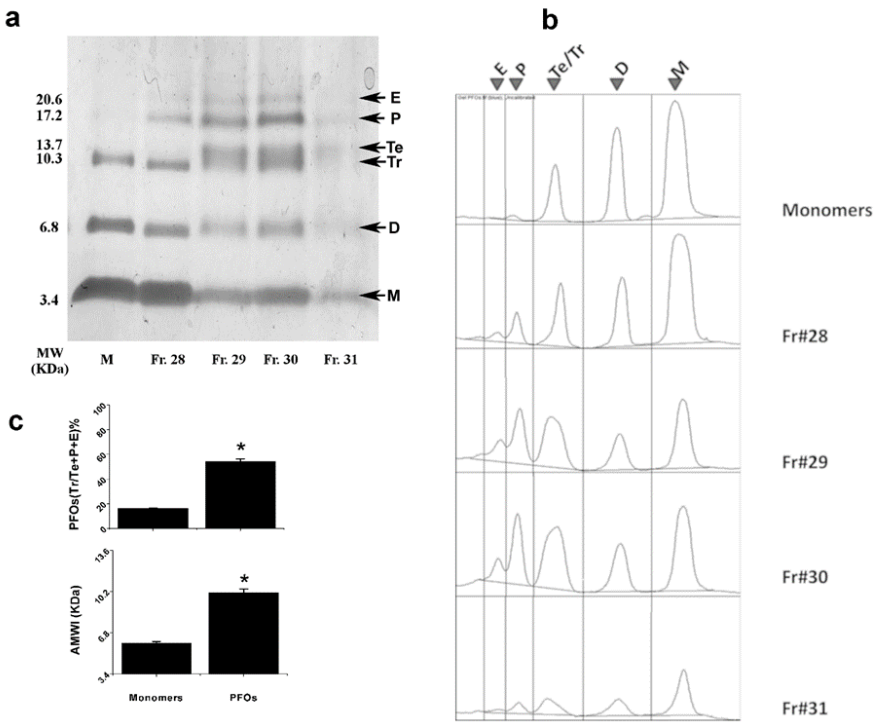

Figure 4- (a) the Tricine SDS-PAGE characterization of the peak fractions. (b) the Gel lane densitometry of the 28,29,30 and 31st fractions (V_e=23.80, 24.65, 25.50, 26.35 mL) enriched in trimers, tetramers, and hexamers, compared to native Monomers-enriched sample containing also dimers and trimers. M: monomers, D: dimers, Te/Tr: trimers-tetramers, P: pentamers, E: Hexamers. (c) the Average molecular weight index and PFOs percentage index for the 29th fraction reported in table 1[42].

In the case of PFOs (fractions 29th and 30th), the gel analysis demonstrated an upwards-shifted pattern as compared to the Monomers

sample, where dimers and trimers were also present. A strong enhancement of the aggregated species, such as tetramers, pentamers, and hexamers, was observed.

To better analyze this trend, based on Gel densitometry (Fig 4b), we calculated two indexes: i) the *Average Molecular Weight index* (*AMWi*); ii) *trimers+tetramers+pentamers+hexamers percentage (PFOs%)* for PFOs-enriched fractions and Monomer unfractionated samples, summarized in Table 1[42].

Table 1- gel densitometry characterization of the SEC peak fractions.

MW (KDa)						
		Monomers	**FR.28**	**FR.29**	**FR.30**	**FR.31**
20,6	Hexamers	22,54	740,16	1828,36	1685,06	308,85
17,2	Pentamers	328,21	1885,18	4660,79	5099,96	898,06
‡12	Tetramers-Trimers	4129,91	4630,23	6919,13	8523,54	1933,62
6,8	Dimers	7519,91	5516,98	3582,10	4828,81	1994,74
3,4	Monomers	15215,90	15417,44	6834,47	9432,42	4134,93
		PFOs%	**PFOs%**	**PFOs%**	**PFOs%**	**PFOs%**
		16,5	25,7	56,3	51,8	33,9
		AMWI	**AMWI**	**AMWI**	**AMWI**	**AMWI**
		5,83	6,85	10,43	9,79	7,84

Results relative to the 29th and 30th fractions (V_e=24.65 and 25.50 mL-see Fig. 4c and Table 1), gave *AMWi=10.0 KDa* for sCT PFOs, which is close to trimer molecular weights (10.2 KDa), while *AMWi=5.8 KDa* for native unfractionated Monomers, which is between Monomer and dimer molecular weights (3.4 KDa and 6.8 KDa, respectively). The percentages of trimers, tetramers, pentamers, and hexamers rises from about 16.5 % for Monomer- to 56.3 % for PFOs-enriched samples. We noticed that, even if monomeric species were overexpressed in the Monomer-enriched samples, dimers and trimers were always present (Fig. 4a).

We would like to underline that, by using sCT we did not obtain aggregates of molecular weight higher than hexamers. As reported earlier, unlike other members of the amyloid family, sCT presents a very low aggregation rate with the longest aggregation lag-phase among CT variants[44]. This raises the possibility to produce stable PFOs-enriched samples made of known aggregates to be tested directly onto the cells.

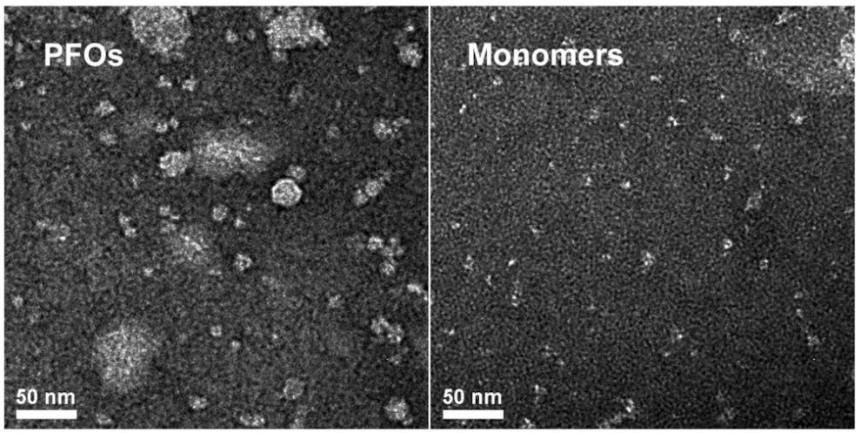

Figure 5 – High-resolution EF-TEM images relative to PFOs (29th fraction) and Monomers. (Bar 50nm)[42].

The Energy Filtered-Transmission Electron Microscopy (EF-TEM) micrographs relative to the central fraction (29th fraction) of the PFOs peak, together with images relative to the Monomer-enriched sample are presented in Fig. 5. Notably, PFOs appeared as particles of 10±3 nm, not perfectly spherical and sometimes characterized by well-defined or incomplete hexagonal shape. Few bigger particles were also present. Conversely, the image of the Monomer-enriched sample revealed the presence of very small dots of about 3±1 nm, likely Monomers, together with clusters of few dots, dimers, and trimers (means of maximum diameters of more than 30 particles per sample type).

PFOs administration to cellular cultures.

Intracellular Ca^{2+}-influx.

We compared the effects induced by sCT PFOs- and Monomer-enriched samples on internal calcium ($[Ca^{2+}]_i$) in 14 DIV hippocampal neurons. PFOs enriched fractions induced an elevated $[Ca^{2+}]_i$ rise, which was maintained after 10 minutes, while sCT Monomers resulted in a fast transient of Ca^{2+}-influx peaking in a minute, coming back to the baseline after 10 minutes (Fig. 6).

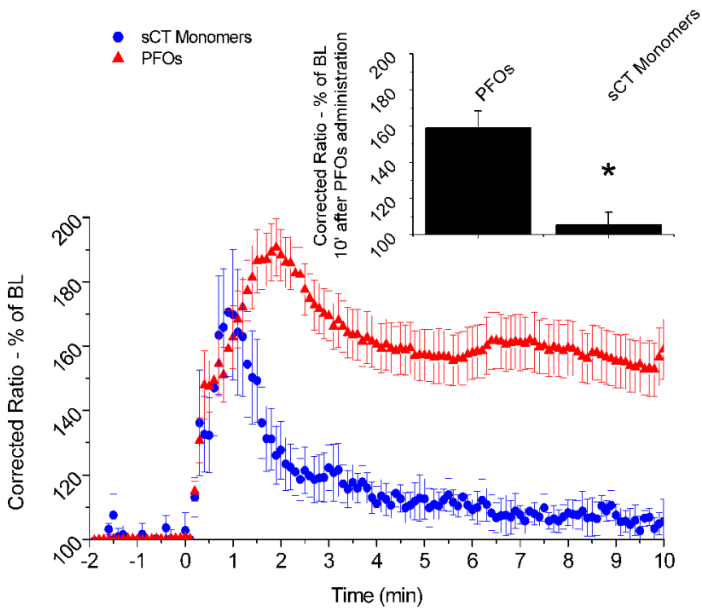

Figure 6-FURA2-AM calcium imaging in 14 DIV hippocampal neurons (n=76 cells) upon of 8 μM sCT PFOs or Monomers infusion in the medium (occurred at zero time). The bar plot represents the intracellular calcium elevation values (mean +SEM), 10 minutes after sample administration[42].

In a previous paper, we reported that the Ca^{2+}-influx was evoked by a spontaneous aggregated mixture of sCT oligomers in 14 DIV hippocampal neurons, which was abolished by disrupting GM1

sialic acid heads by neuraminidase[14]. Thus, we hypothesize that growing levels of this ganglioside would result in the $[Ca^{2+}]_i$ increase. To investigate if the Ca^{2+}-influx depends on the GM1 content, we compared undifferentiated HT22 cells, differentiated HT22 cells, primary hippocampal neuronal cultures from rat hippocampi at 6 DIV and 14 DIV. It is well known that the GM1 content increases with neuronal differentiation degree. We verified this fact in our cells by immunofluorescence (Fig. 10).

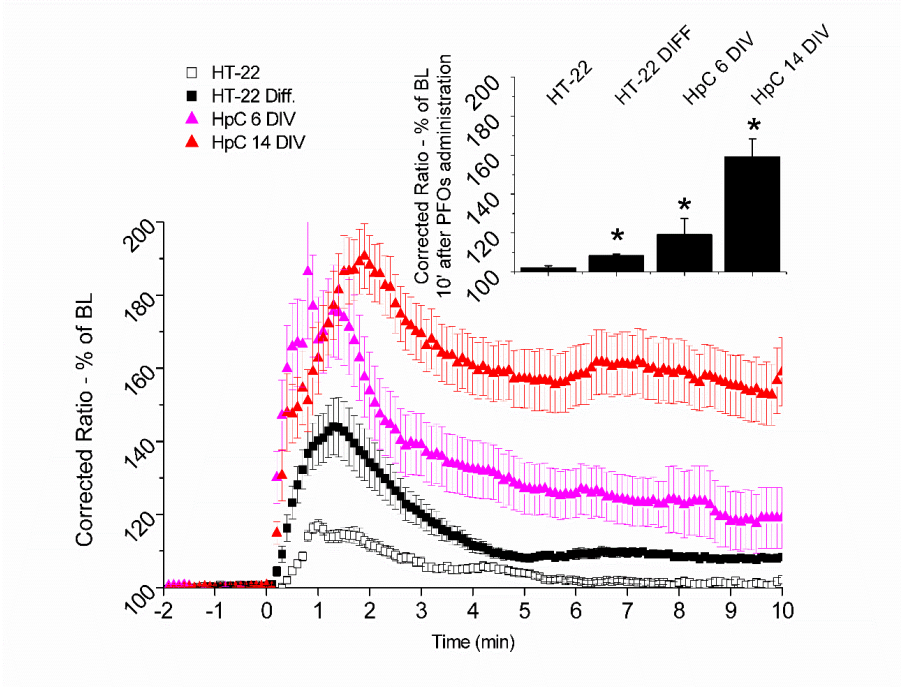

Figure 7 – Differences in the intracellular calcium elevation induced by 8 µM sCT PFOs administrated in the bath., in hippocampal neurons at DIV 14 (n=76 cells), DIV 6 (n=73 cells) as well as in differentiated HT-22 (n=140) and in HT-22 (n=659) cells. Bar plot represents the intracellular calcium elevation values (Corrected ratio percentage over the baseline -mean + SEM), after 10 minutes[42].

As depicted in Fig. 7, significant differences were obtained between all groups. As can be observed, the shape and intensity of the curves changed with the differentiation degree. The high and sustained

Ca^{2+}-influx of 14 DIV hippocampal neurons was reduced for 6 DIV neurons. The shape was maintained in the first minutes, but the plateau reached in the second part was more than halved. HT22 DIFF cells gave rise to less intense signals, with a shape very similar to that of 6 DIV neurons. Finally, we note that undifferentiated HT22 cells showed the smallest Ca^{2+}-influx, vanishing after about 6 minutes.

Summarizing, we noticed a strong correlation between $[Ca^{2+}]_i$ signal maintained after 10 minutes and cell differentiation degree (inset of Fig. 7).

To investigate the nature of the Ca^{2+}-influx we pre-treated 14 DIV neurons with MK801, a specific blocker for NMDAR and with Verapamil, a VDCC blocker.

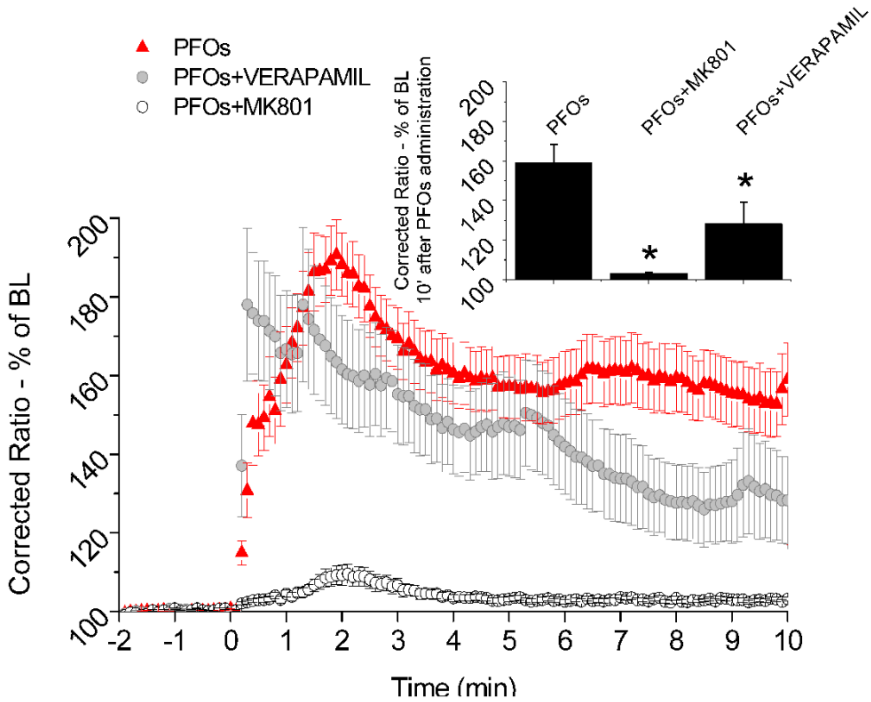

Figure 8 – Differences in the intracellular calcium elevation induced by 8 µM sCT PFOs administrated in the bath., in hippocampal neurons at DIV 14 (n=76 cells), DIV 6 (n=73 cells) as well as in differentiated HT-22 (n=140) and in HT-22 (n=659) cells. Bar plot represents the

intracellular calcium elevation values (Corrected ratio percentage over the baseline -mean + SEM), after 10 minutes[42].

Results (Fig. 8) indicated that, after treatment with MK801, the $[Ca^{2+}]_i$ increase was reduced to a small and transitory peak, suggesting that the strong and maintained Ca^{2+}-influx of the 14 DIV neurons was due to the NMDARs. Conversely, we found a slight dependence on voltage-activated Ca^{2+} channels, since their specific blocker (Verapamil) determined only a small decrease in the PFOs-evoked response.

We want to stress the similarity in shape and intensity between the peak obtained with undifferentiated HT22 cells (Fig. 7) and the one observed with 14 DIV neurons in the presence of MK801 (Fig. 8) where NMDARs were inhibited. This similarity suggests that a mechanism different from NMDAR activation was in part responsible for $[Ca^{2+}]_i$ increase. Notably, as pointed out by He *et al.*, these channels were missing in the HT22 cells[52]. To verify this important issue, we treated both HT22 and HT22 DIFF with the agonist NMDA, monitoring the induced Ca^{2+}-influx. Results clearly showed that Ca^{2+}-influx was absent in HT22 cells, confirming the lack of NMDARs (Fig. 9) and demonstrating that the small peak induced by sCT PFOs must be due to a different mechanism.

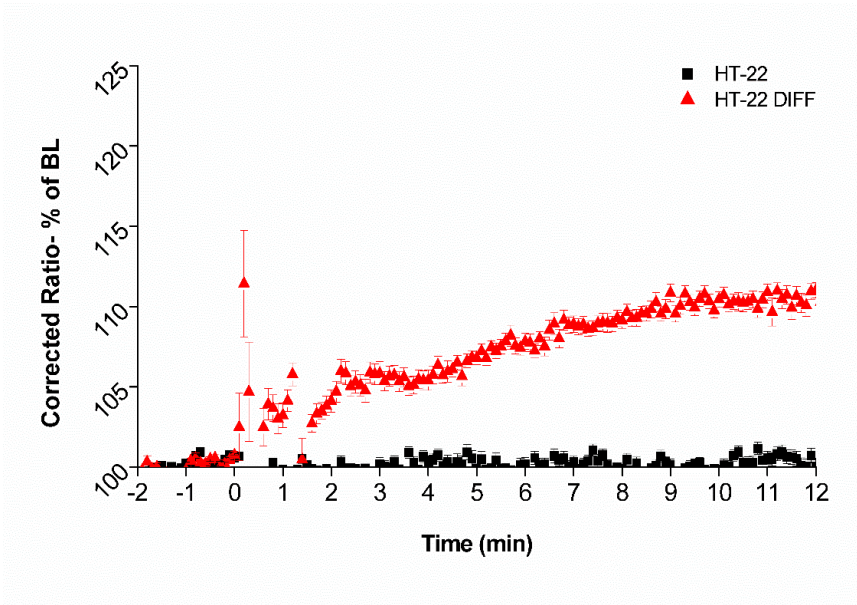

Figure 9 - FURA2-AM calcium imaging in differentiated HT-22 vs undifferentiated HT-22 (n=76 cells) upon of 10 µM NMDA infusion in the medium (at time zero). The bar plot represents the intracellular calcium elevation values (mean +SEM), 10 minutes after sample administration[42].

NMDA induced a gradual raising of $[Ca^{2+}]_i$ in HT22 DIFF, demonstrating that, as reported by He *et al.*, the differentiation process leads to the expression of the NMDARs[52]. However, the shape of the Ca^{2+}-influx induced by NMDA in HT22 DIFF (Fig. 9) was very different from that induced by sCT PFOs, lacking the transitory features occurring in the first minutes and characterized by a plateau value reached after 10 minutes, of the same intensity of the plateau reached with sCT PFOs (Fig. 7a). This suggests that NMDARs were responsible for the Ca^{2+}-influx obtained at the steady-state, in agreement with the conclusion drawn in the case of 14 DIV neurons pre-treated with MK801 (Fig.8).

Finally, to investigate the possible correlation between Ca^{2+}-influx and GM1 expression, we examined by fluorescence microscopy the membrane distribution of GM1 in all cell types, by using fluorescence-labelled CTβ known to selectively bind the GM1 sialic acid heads. In HT22 cells, images showed the characteristic dotted distribution and the increase of GM1 expression due to differentiation (Fig. 10 upper panel) while, in hippocampal cultures, GM1 was evenly distributed throughout the plasma membranes (Fig. 10, lower panel) and the GM1 content further increased upon differentiation (lower panel). We conclude that a correlation exists between Ca^{2+}-influx and GM1 expression.

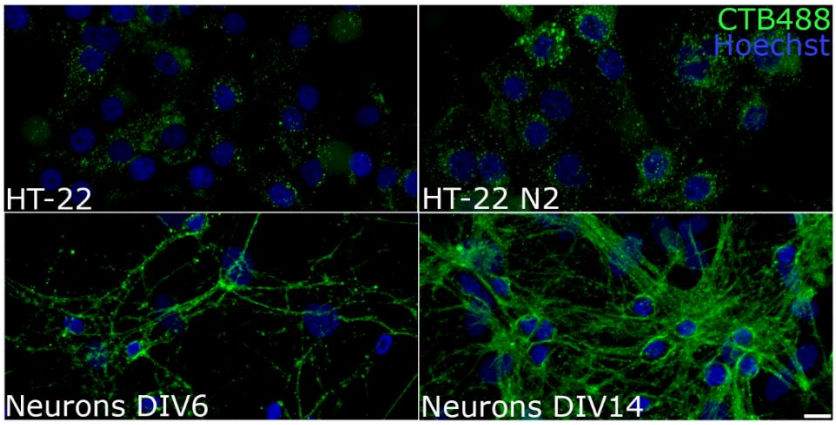

Figure 10-Immunofluorescence microscopy of the GM1-raft distribution in different cell types at an increasing stage of differentiation: the GM1 ganglioside is specifically stained by fluorescent-cholera toxin beta subunit (green). Cell nuclei are counterstained by Hoechst 33258 (blue). Bar = 20 μm.

Summarizing, we provide evidence that sCT PFOs evoked strong and sustained intracellular Ca^{2+}-influx mediated by NMDARs and that this behaviour was correlated with the GM1 expression. In the absence of NMDARs or with these channels blocked, and with few GM1 (undifferentiated HT22) a small but detectable Ca^{2+}-influx was still observed[42].

Cell viability.

To clarify if neurotoxicity is correlated to the aggregation state of sCT, we studied the dose-response relationship of PFOs- and Monomers-enriched solutions in HT22 DIFF cells, after 24 hours. Results clearly showed that only PFOs-enriched solutions induced cell viability reduction (about 10%) while Monomers-enriched solutions were harmless (Fig. 11).

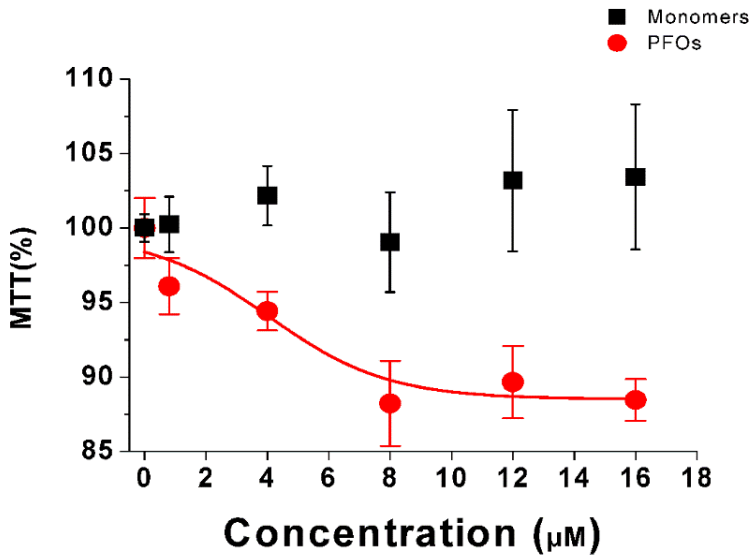

Figure 11- Dose-response relationship of the cellular viability induced by sCT PFOs (red) and Monomers rich solutions (black) in HT-22 differentiated cells. Cellular viability was evaluated by MTT assay and expressed as the percentage over controls (mean ±SEM). Then sigmoidal regression was calculated[42].

Notably, the same result was obtained with 14 DIV hippocampal neurons (Fig.12). Based on these results we decided to perform all viability experiments at 8 μM concentration. We noticed that cell viability reduction depended on the cell differentiation degree. As reported in Fig. 12c, it was higher in hippocampal neurons (about

25%) than in HT22 DIFF. Notably, undifferentiated HT22 cells didn't reach significant toxicity.

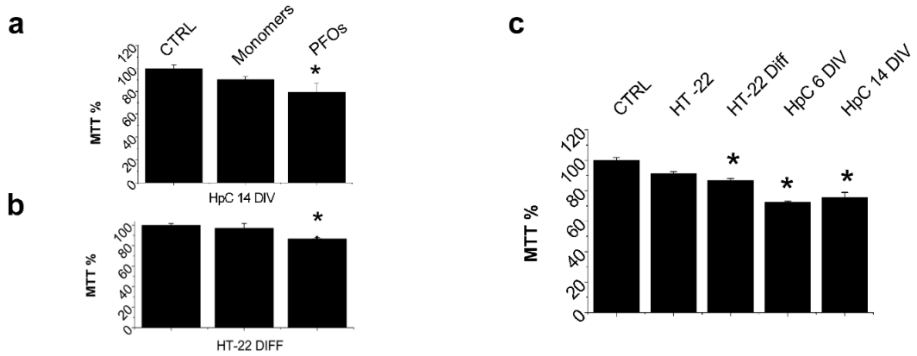

Figure 12 - Cell viability (MTT assay). PFOs- but not Monomer-enriched solutions reduced cell viability in both .(a) 14 DIV primary hippocampal neurons (CTRL n = 20 wells from N = 4 experiments, Monomers n = 17 wells from N = 3 experiments, PFOs n = 31 wells from N = 3 experiments) and (b) HT22 DIFF cells (CTRL n = 51 wells from N = 9 experiments, Monomers n = 14 wells from N = 4 experiments, PFOs n = 192 wells from N = 38 experiments), after 24 h of incubation. (c) This effect depends upon the cellar differentiation stage (thus in GM1 expression) and fade in undifferentiated HT22 cells (CTRL n = 135wells from N = 25 experiments, HT22 n = 194 wells from N = 8 experiments, HT22 DIFF n = 192 wells from N = 38 experiments, HpC 6 DIV n = 31 wells from N = 3 experiments, HpC 14 DIV n = 31 wells from N = 3 experiments). CTRL is relative to the untreated specific cell[42].

Finally, we noted that the loss of viability was not time-dependent, since after 10, 100 minutes and 24 hours of treatment, the same reduction was observed in 14 DIV hippocampal neurons (Fig. 4c).

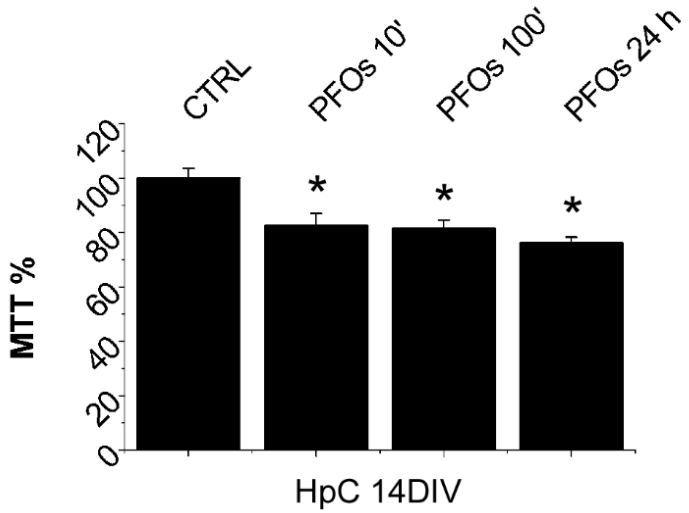

Figure 13- Cell viability (MTT assay) was reduced even after only 10 min of incubation with PFOs with 14 DIV primary hippocampal neurons (CTRL, 10 min, 100 min and 24 h n = 10 wells from N = 3 experiments). CTRL is relative to the untreated specific cell (a–d) while in (b) to cell kind normalized to 100%. With "control" we intend "vehicle-treated" samples[42].

Therefore, we investigated whether a correlation existed between the $[Ca^{2+}]_i$ increase and reduction in cell viability. In good agreement with the Ca^{2+}-influx experiments, MTT results clearly showed a direct relationship between cell differentiation and/or GM1 expression and PFOs induced neurotoxicity. As in the case of Ca^{2+}-influx, before PFOs administration we pre-treated our cell cultures with MK801 and Verapamil (Fig. 14).

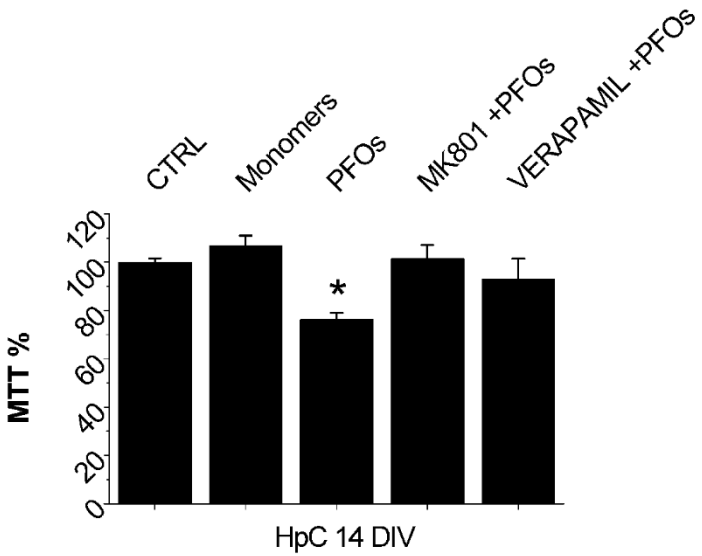

Figure 14 - Cell viability (MTT assay) demonstrates that the Ca2+-channel blockers (MK801 and Verapamil) were able to protect against the PFOs neurotoxicity (CTRL n = 15 wells from N = 3 experiments, Monomers n = 12 wells from N = 3 experiments, PFOs n = 40 wells from N = 3 experiments, MK801 + PFOs and Verapamil + PFOs n = 11 wells from N = 3 experiments). (a–d) while in (b) to cell kind normalized to 100%. With "control" we intend "vehicle-treated" samples[42]

In agreement with Ca^{2+}-influx results, we found that these blockers fully reverted neurotoxicity. This indicates a direct relationship between neurotoxicity and levels of $[Ca^{2+}]_i$ reached after 10 minutes and more. To confirm that the reduction of cell viability observed with MTT assay was mainly due to the reduction of neuronal cells instead of glia, we performed immunofluorescence analysis and TUNEL assay of PFOs treated hippocampal cultures (Fig. 15).

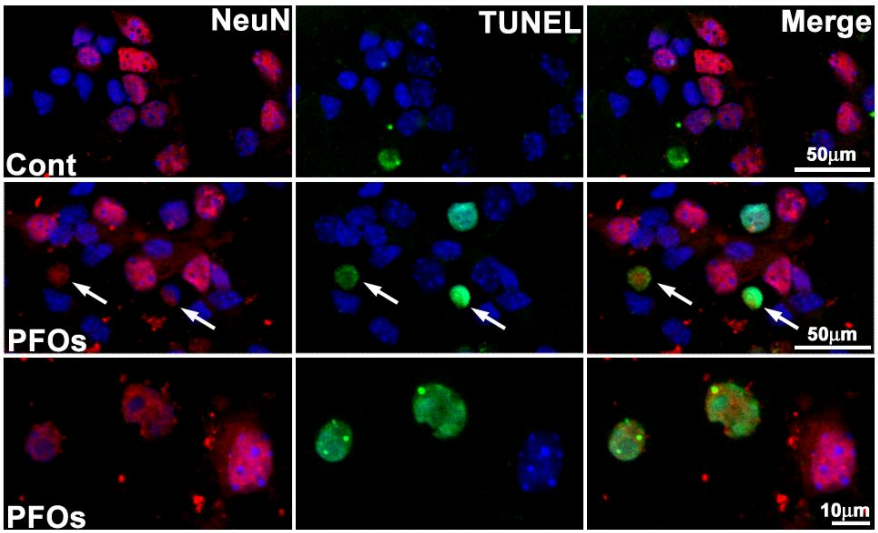

Figure 15- The treatment with sCT PFOs induces apoptosis in primary hippocampal cultures. Hippocampal cultures at DIV 14 were immune-stained for Neurons (NeuN- red), apoptosis was evaluated by the TUNEL assay (green). After treatment with PFOs, we observed an increase in apoptotic nuclei that appear to colocalize with NeuN (arrows). The second row is at higher magnification. Nuclei were counterstained with Hoechst 33258 (blue)[42].

Results showed reduced expression of NeuN positive cells, indicating that the damaged cells were neurons. Moreover, the colocalization of the NeuN and the TUNEL assay confirmed that PFOs treatment induced apoptosis in neurons.

Acute PFOs administration to brain slices.

Synaptic plasticity. Over the last decades, the link between oligomers neurotoxicity and synaptic plasticity impairments have been investigated for Aβ[6,30,31,45,49,51,53-57]. As well known, Aβ is an unstable protein and, in agreement with Benilova *et al.*, the sample changed along different preparation making interpretation and direct comparison of data between different research groups very difficult[5]. At present, any attempt to test the effects of amyloid native PFOs and stable Monomers during the experiment on synaptic plasticity hasn't been obtained yet. Herein, we investigated the effects of native samples, as intended in the introduction[3,4], on synaptic plasticity. PFOs and Monomers were diluted in carboxygenate Artificial Cerebro Spinal Fluid (ACSF) at a final concentration of about 3 μM and used to superfuse mouse hippocampal slices.

sCT PFOs-enriched samples fully abrogated LTP in hippocampal slices, 80 minutes after tetanus, while native Monomer-enriched solutions did not affect LTP even when compared to control (Fig. 16). Interestingly, LTP reduction in the case of sCT PFOs was very similar to that reported for Aβ[6]. However, for the first time to our knowledge, we report significant differences between effects induced by sCT native amyloid PFOs- and Monomer-enriched solutions.

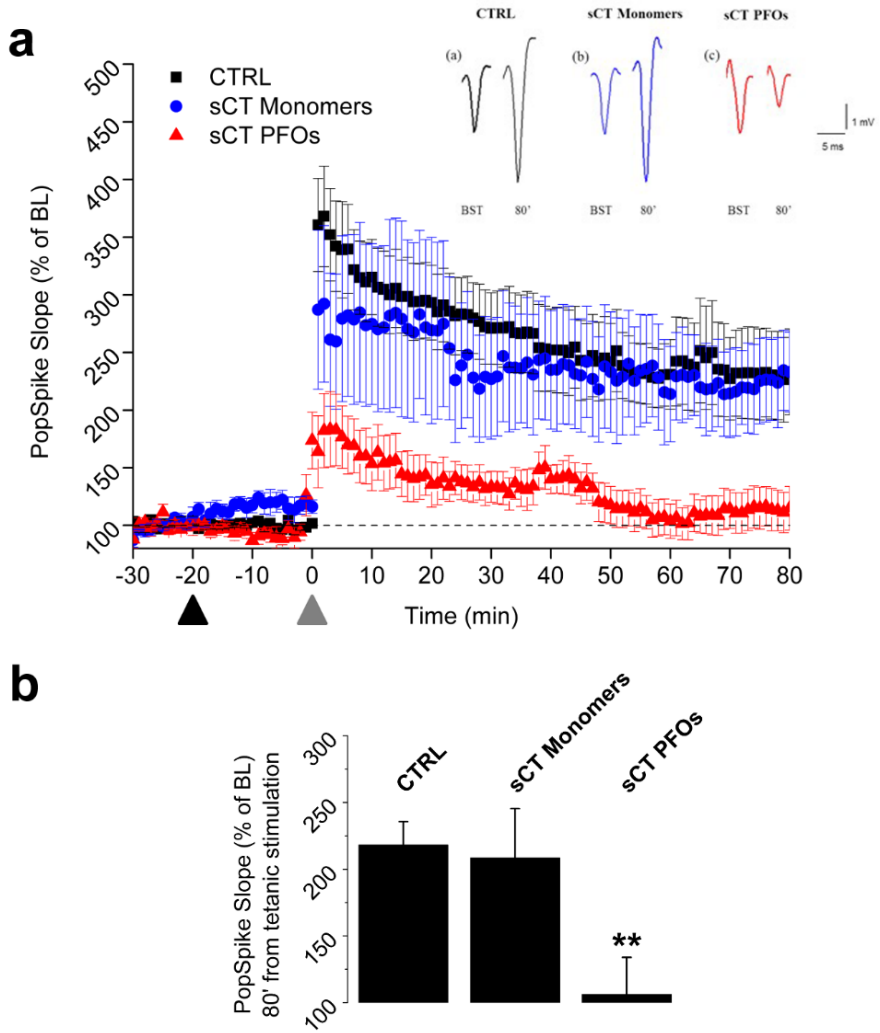

Figure 16 - Long-Term Potentiation results. (a) shows spectra relative to LTP induced in hippocampal brain slices by sCT PFOs- (n = 6) and Monomer-enriched solutions (n = 6), compared to untreated samples (CTRL) (n = 6). The black arrow represents the sample administration while grey arrow the tetanic stimulation (signals are reported in the inset of a). (b) shows the level reached after 80 min from the tetanic stimulation. With "control" we intend "vehicle-treated" samples[42].

Immunofluorescence and Western blotting for synaptic proteins. to evaluate whether the altered activity of LTP was correlated with an impairment of synaptic structures[58,59] and loss of dendritic spines[60], we studied the expression of a pivotal post-synaptic protein such as Post Synaptic Densities protein-95 (PSD-95) and the pre-synaptic synaptophysin, a component of synaptic vesicles, using immunofluorescence confocal microscopy (Fig. 17) on the same brain sections recorded in LTP.

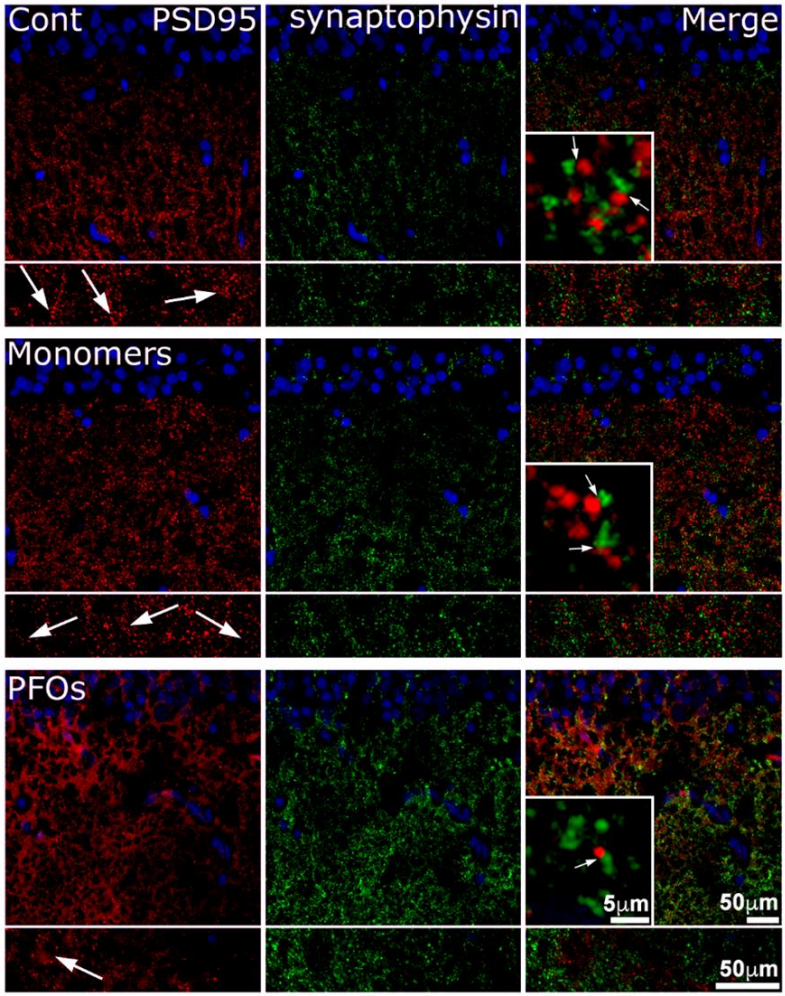

Figure 17-Pre-and post-synaptic immunolabelling) of treated hippocampal slices, revealed that sCT PFOs reduced PSD-95 levels (red), leaving synaptophysin expression almost unchanged (green). Nuclei (blue) were counterstained with Hoechst 33258. Arrows highlight, at 40x magnification, a significant loss in PSD-95 positive dots, following PFOs administration, while treatment with Monomer-enriched solution let postsynaptic densities almost unchanged[42].

The immunofluorescence showed a loss in PSD-95 positive presynaptic structures concerning controls, while the synaptophysin signals were unmodified.

To better analyze this issue, we performed WB analysis on the same hippocampal slices incubated with sCT PFOs (Fig. 18), to quantify protein expression. Results demonstrated a significant decrease in the PSD-95 expression respect to untreated slices (Fig. 18b). Under the same conditions, the levels of synaptophysin remained unmodified (Fig. 18c).

Notably, in agreement with LTP results, our findings showed that the treatment with sCT Monomer-enriched solutions did not modify the levels of these proteins (Fig. 17-18).

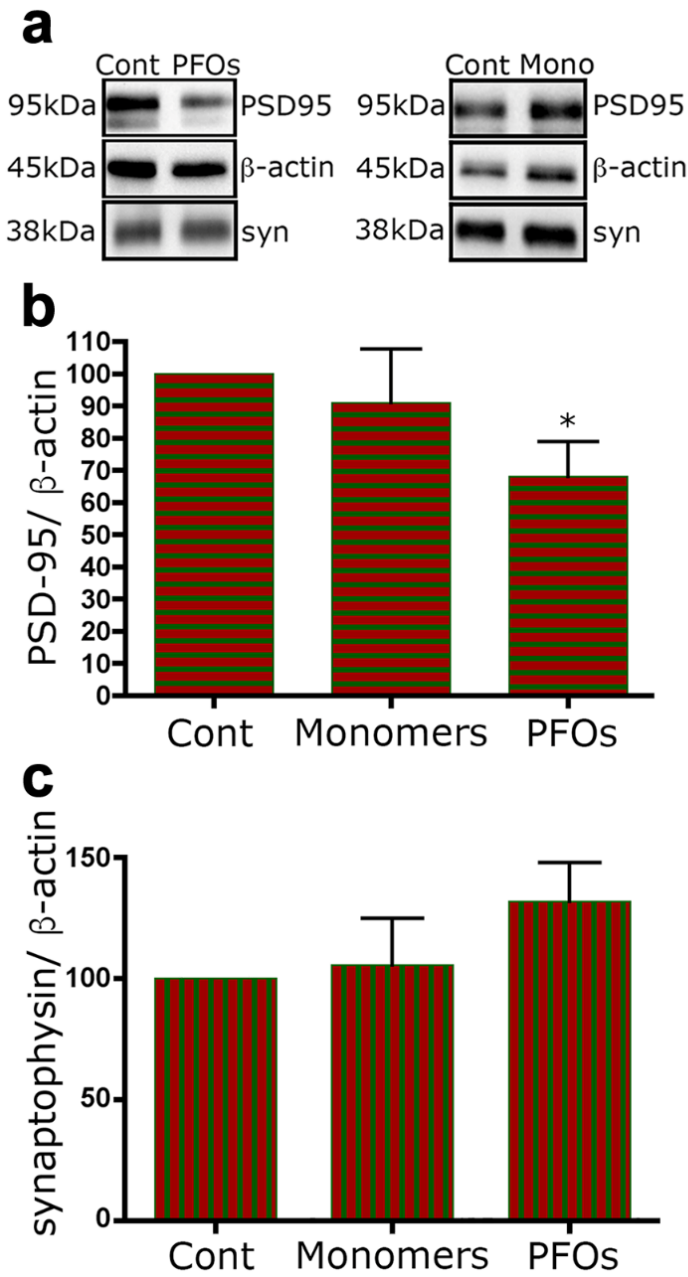
a
Cont PFOs
95kDa
PSD95
45kDa
β-actin
38kDa
syn
Cont Mono
95kDa
PSD95
45kDa
β-actin
38kDa
syn
b
PSD-95/ β-actin
110
100
90
80
70
60
50
40
30
20
10
0
*
Cont
Monomers
PFOs
c
synaptophysin/ β-actin
150
100
50
0
Cont
Monomers
PFOs

Figure 18- (a) representative WB analysis in hippocampal slices: treated with sCT PFOs- or Monomer-enriched solutions. Bar plots represent mean ± SEM from n=4 independent experiments assessing (a) PSD-95 expression- and (b) synaptophysin expression- normalized for β actin. A significantly decreased level of PSD-95 is observed after treatments with sCT PFOs. (p-value < 0.05 Mann–Whitney U test), but not with Monomers. While any significant difference in synaptophysin expression was obtained against controls. WB analysis confirmed the results obtained with Immunofluorescence analysis[42].

Inside out- patch-clamp recordings.

To evaluate whether sCT PFOs administration would result in the amyloid pores formation[33] we performed inside-out patch-clamp recordings (Fig.19), in voltage-clamp mode, on membranes excised from primary hippocampal neurons. In this configuration, it is possible to analyze, at a very high signal to noise ratio, currents arising from ionic channels or pore-like structures, with a "single-channel" resolution[45].

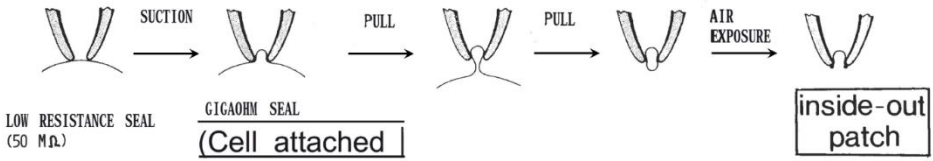

*Figure 19- excised patch-clamp in **inside-out** configuration. Once the giga-ohm seal is achieved, the patch pipette is slowly retracted from the cell, resulting in the formation of a small vesicle. Once the pipette tip is exposed to the air, the outer portion of the vesicle rapidly break-up. Then the pipette is soaked again in the bath, exposing its intracellular side toward the external solution. Modified from* [45]

As expected, in normal conditions, inside-out patch of neuronal membranes displays, the activation of several endogenous conductances, at a single-channel resolution, displaying voltage dependence and specific gating properties (Fig. 20).

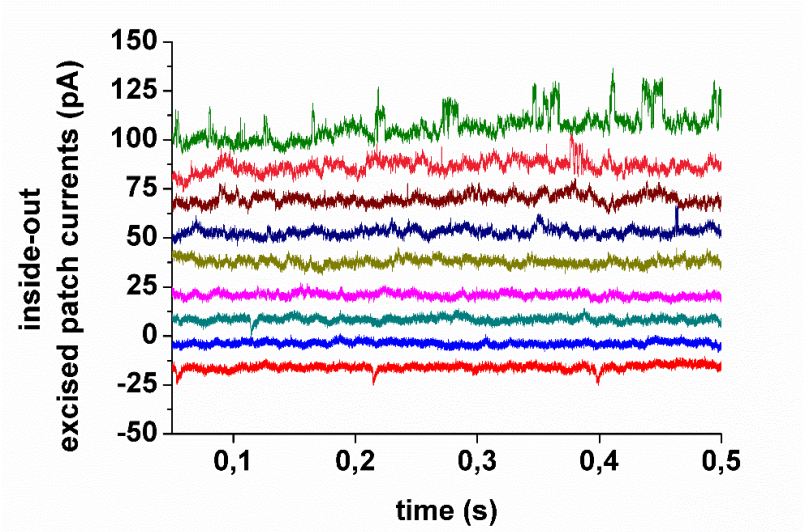

Figure 20- "single-channel" currents recorded from an Excised patch of neuronal membranes, evoked upon depolarizing steps of voltage from -30 to +90mV.

First, we blocked them, adding specific drug blockers in extracellular solution (1µM TTX, 10mM TEA, 100µM Bicuculline, 10µM CNQX, 100µM APV), to obtain current responses, independent from endogenous channels activations.

Then, according to the protocol of Bode and colleagues, patch pipettes were backfilled with the same symmetrical solution (see methods) containing samples (sCT PFOs or Monomers, at 8µM). In the pipette, samples were free to diffuse facing the extracellular side of the excised patch. Transmembrane currents were measured (Fig. 21) by clamping the patch at a series of voltage potentials between -60 and +60 mV[33]. This sweep was repeated one a minute for about 50 times. While, in sample-free experiments (CTRL), the transmembrane conductances remained steady along with the trials, in the case of samples-backfilled patches, after a variable lag of time spanning from 5 to 10 minutes, increased transmembrane conductances occurred and were maintained throughout the experiments. In all cases, R-series was always under 20MΩ.

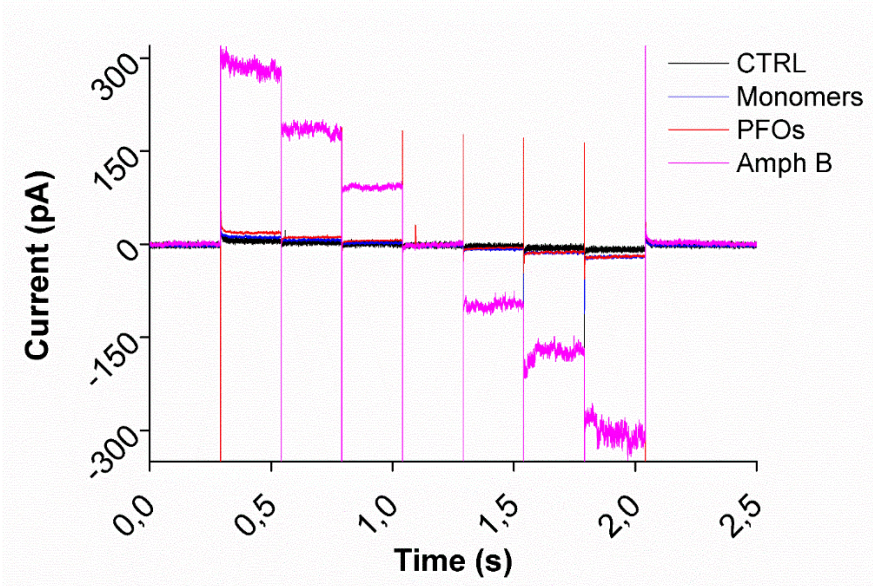

Figure 21- transmembrane currents from an excised membrane patch, in inside-out configuration. Patch of membrane were clamped with a series of voltage potentials whose amplitude in mV was:0, +60, +40, +20, 0, -20, -40, -60, 0. Pipette tips were filled with about a millimetre of an extracellular solution containing drug blockers, free from samples to gain a time delay for sealing and excising the patch. Pipettes were backfilled with the same solution added with Monomers (blue traces) or PFOs (Red traces) at a final concentration of 8 µM or with Amphotericin B (Magenta traces) 150 µg/mL.

As depicted in Fig. 21, sCT PFOs administration resulted in a doubling of the transmembrane currents with respect to sCT Monomers. To get a better idea of what we found, we repeated the experiments using the well-known ionophore Amphotericin-B (150 µg/mL) instead, as a positive control. The effects of Amphotericin B were about 10 folds higher respect to those seen with Monomers and PFOs (Fig. 22). The trial duration was about 50 minutes, the last 15 traces of the experiments were averaged and plotted against the respective voltages they were clamped. Notably, all these currents presented a linear voltage-current

relationship (Fig. 22). Conductances of the pores, obtained from the I-V relationship slopes, were expressed in pS [1S=1A/1V].

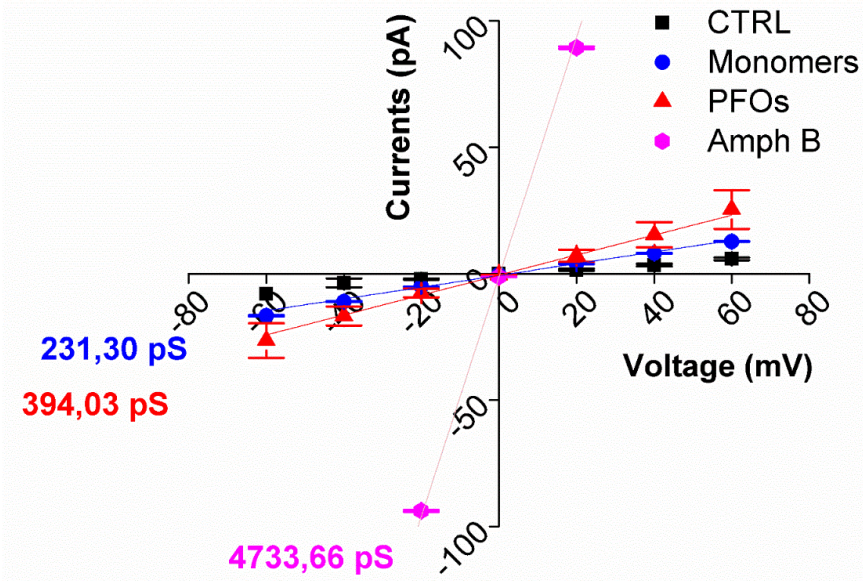

Figure 22 - current-voltage relationship for an excised patch of neuronal membranes. Average transmembrane steady-state currents were correlated with respective voltage potentials. Linear regression was applied to data. Controls (black traces), Monomers (blue traces), PFOs (Red traces) and Amphotericin B (Magenta traces). Conductances were calculated as the slope of the linear regression and expressed in pS.

Although these last results are preliminary, together all this body of evidence agrees with the idea that PFOs drive the formation of small “amyloid pores” with very low conductances.

Spontaneous miniature Excitatory Posts-Synaptic Currents.

Mature neuronal cultures make thousands of mutual synaptic connections. During active transmission, synaptic vesicles are synchronously released from presynaptic endings by the activation of voltage-dependent calcium channels, following the action potential arrival. On the contrary, at resting conditions neurotransmitter release, follows a stochastic route. Therefore, for each synapse, it is very likely that some quanta of neurotransmitter might be released, also at rest.

The small currents evoked by these spontaneously released quanta on the postsynaptic neurons, are named “miniature Excitatory Post Synaptic Currents” (mEPSCs) or “minis” and can be measured, in absence of any other stimulation, by patch clamping the postsynaptic neurons (Fig. 23), in whole-cell mode (Fig. 24).

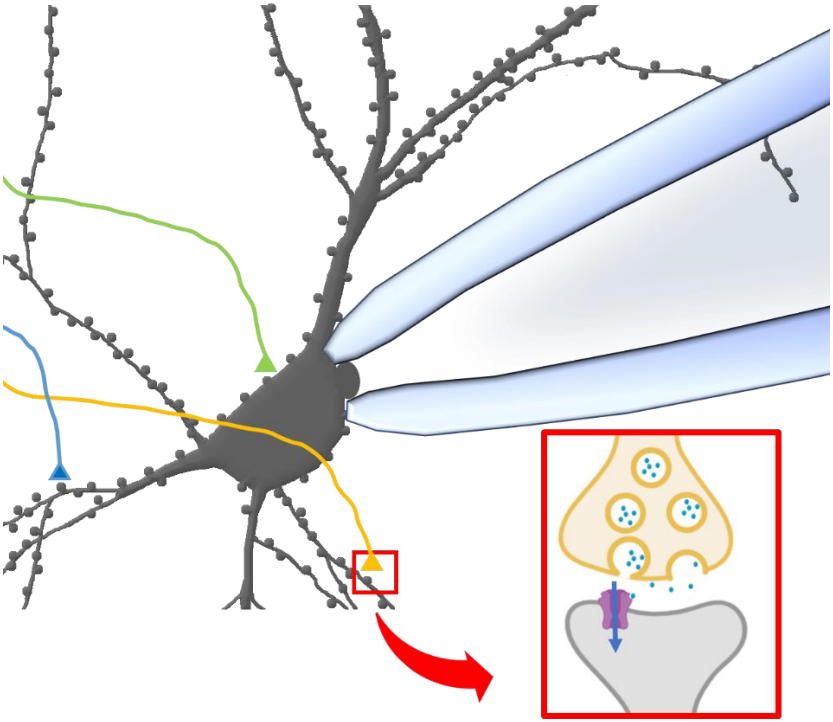

Figure 23- Schematic of miniature Excitatory Postsynaptic Currents (mEPSCs) recorded from a cultured hippocampal neuron. For each synapse (dots along with soma, axon, and neurites), a spontaneous release occurs, in the presynaptic terminals, at resting conditions. Three presynaptic afferences are depicted in green, blue and yellow. Once, a single quantum of neurotransmitters (blue dots in the inset) is released and reaches the postsynaptic terminal a miniature Excitatory Postsynaptic Current, flows through the activated receptors into the postsynaptic neurons. These miniature currents can be measured by patch clamping the postsynaptic neurons, at the holding potential.

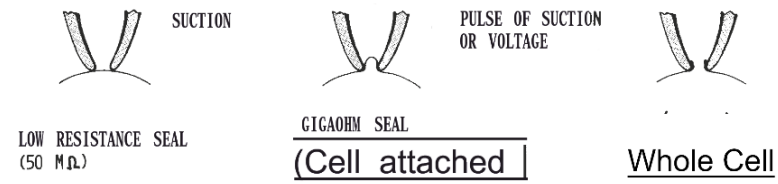

Figure 24 - Once the giga-ohm seal configuration is achieved, a deep pulse of suction allows to break the patch and to go into the whole cell configuration. Now, all the transmembrane currents are measured by the patch clamp pipette, while the cell is clamped at the selected holding potential. Modified from [45]

Since mEPSCs are very small currents (typically 10 pA), they can be masked by the occurrence of a concomitant action potential or waken by the activity of inhibitory synapses. Thus, to record mEPSCs an action potential blocker (i.e. tetrodotoxin 1 µM), as well as a GABA-A receptors inhibitor (i.e. Bicuculline10 µM) must be added in the medium. Generally, the magnitude of mEPSCs is proportional to the number of quanta released and to the number of receptors that can be activated from that neurotransmitters. But this is true only in the absence of long-term potentiation effects, thus with the purpose of successfully record mEPSCs in glutamatergic neurons also an inhibitor of NMDARs needs to be used.

Based on the idea that PFOs administration would result in neuronal membrane permeabilization, we asked whether this membrane leakage might be responsible for the synaptic strength impairment, seen in LTP experiments and intracellular calcium elevation, via unbalancing of the neurotransmitters release mechanisms.
To address the effects of amyloid pore formation onto the basal release, we performed recordings of the spontaneous mEPSCs, on the same neuronal cultures in control conditions and following sCT PFOs administration in the bath. As depicted in (Fig. 25), we found that PFOs induced a deep alteration in amplitude and frequency of spontaneous mEPSCs, demonstrating a clear effect on synaptic release.

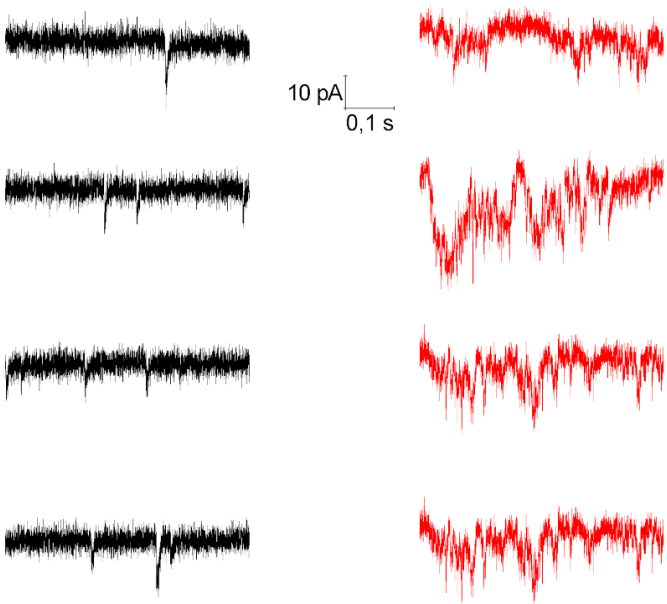

Figure 25- spontaneous mEPSCs in primary hippocampal neurons at 14 DIV, before (black traces) and after (Red traces) sCT PFOs administration in the bath. Whole-cell recordings were made in the presence of 1µM TTX, 10 µM APV and 50 µM Bicuculline. Neurons were clamped at the holding potential. After 10minutes of adaptation, PFOs were administered in the bath.

We speculate that a sustained/ abnormal quantal release would be responsible for the synaptic failure, hence in LTP depression.

To date, these last results are still in progress, but if confirmed this data could produce the final proof of a new amyloid neurotoxic mechanism where amyloid pores formation drives the unbalancing of neurotransmitter release and a consequent "amyloid-mediated-excitotoxicity".

Discussion

Our results proved that sCT was a useful candidate to prepare native PFOs- or Monomers-enriched samples without any stabilization procedure[9]. Due to its very low aggregation rate, PFOs samples were stable during experiments and rich in aggregates not greater than hexamers. These properties allowed us to overcome difficulties highlighted by Benilova *et al.* in the identification of the amyloid structures responsible for neurotoxicity[5]. Moreover, the sCT PFOs morphology and, more important, the biological effects they induced were very similar to those reported for toxic Aβ oligomers[3,5].

We demonstrated[42] that native soluble sCT PFOs-rich samples, composed of tetramers, pentamers, and hexamers but not species of higher molecular weights, were able to induce a sustained Ca^{2+}-influx in cells expressing GM1 lipid-RAFT (Fig. 7 and Fig. 10). Moreover, we found that in each cell type, the steady-state of this Ca^{2+}-influx was related to the magnitude of GM1 expression, though, the ion influx was dependent on multiple mechanisms, mainly driven by the activation of NMDARs[35] and in a lesser way by presynaptic voltage-dependent calcium channels (Fig.8). Notably, GM1 and NMDARs expression seems to be somewhat covariant. This makes sense since the more NMDARs are expressed, the more receptors-recipient structures (GM1 positive lipid-RAFT) are needed in the cellular membranes. Interestingly, when NMDARs were blocked by MK801, in 14 DIV neurons a small residual NMDAR-independent component, of Ca^{2+}-influx was still observed (Fig. 8). In our opinion, this component could be consequent to the formation of amyloid-pores. We base this hypothesis on our data relative to undifferentiated HT22 cells (Fig. 7). As shown by He *et al.*, these cells do not express cholinergic and glutamatergic receptors, and in particular NMDARs[52]. We carefully verified this point by treating cells with NMDA and observing any Ca^{2+}-influx (Fig. 9). PFOs were able to induce a Ca^{2+}-influx transitory peak even in undifferentiated HT22, but the steady-state value of this calcium influx rapidly come back to the baseline (Fig. 9). In these cells, we

found a poor but significant expression in GM1-lipid RAFT, even in absence of NMDARs. On the other hand, in primary neurons the steady-state magnitude of the residual component obtained with MK801 was higher; because neurons are expressing much more GM1, thus offering more nucleation sites to the PFOs, producing many more amyloid pores. Finally, voltage-dependent calcium channels activation also implies possible presynaptic effects. All these observations agree to the hypothesis that the observed Ca^{2+}-influx could be consequent to amyloid pore formation.

Several groups proposed that the presence of GM1 is necessary for pores formation[13,55-57]. Here we report that undifferentiated HT22 cells expressed low but detectable, levels of GM1 (Fig. 10). Therefore, we hypothesize that in these cells a few amyloid pores can be formed, determining a weak and transitory Ca^{2+}-influx, which is insufficient, *per se,* to affect cell viability (Fig. 7). Notably, we found the same peak in 14 DIV primary neurons pre-treated with MK801, where NMDARs were blocked (Fig. 8).

It is worth noting what happened working with HT22 DIFF cells, which express both higher levels of GM1 (Fig. 10) and glutamatergic receptors[52] (Fig. 9). In this situation, the Ca^{2+}-influx was more than doubled in intensity and remained sustained beyond 10 minutes (Fig. 9), enough to induce a significant (about 10%) decrease in cell viability (Fig. 11).

In agreement with this hypothesis, when primary neuron cultures (6 DIV, 14 DIV) were analyzed, high GM1 contents (Fig. 10) led to the formation of several amyloid pores, enough to boost up the abnormal activation of the NMDARs previously described in differentiated HT22 cells. In 6 DIV and, more pronounced, in 14 DIV, the Ca^{2+}-influx curves more than doubled those observed in HT22 DIFF (Fig. 7) and a cell viability reduction was about 25% (Fig. 12).

The crucial role played by GM1 in the formation of amyloid pores by PFOs, has been recently highlighted by Hong et al. for Aβ[24]. Furthermore, in a previous paper, we showed that masking GM1 in rat primary hippocampal neurons prevents Ca^{2+}-influx and toxicity induced by spontaneous aggregated mixtures of sCT oligomers[14].

However, the present results[46] indicate that the formation of amyloid pores alone is not enough to explain neurotoxicity and that NMDARs must be involved, as suggested by the protection exerted by MK801. Finally, we note that none of the effects described before was induced by sCT Monomer-enriched samples, containing a minority of dimers and trimers. As proposed by Angelova and Abramov, this can be due to the inability of Monomers to form stable amyloid pores and to switch on the pathological Ca^{2+}-influx and the consequent neurotoxicity[37].

Supporting the pore formation hypothesis, we demonstrated that in the excised patch of neuronal membranes at 14 DIV, upon the blocking of endogenous conductances (including NMDARs), only PFOs while not monomers resulted in the formation of passive conductances (Fig. 21) showing a linear voltage-current relationship (Fig. 22).

Concerning LTP experiments, we showed that sCT PFOs abrogated synaptic plasticity after 100 minutes of treatment while, in good agreement with neurotoxicity results described before, monomer-enriched solutions were ineffective (Fig. 5). Similar results have been reported for aggregates of other amyloid proteins[5,6,30,51,54]. However, in our knowledge, the direct comparison between the effects induced by PFOs and Monomers has been never investigated for sCT.

Interestingly, we provide evidence that cells were damaged after 10 minutes as well as, after 24 hours of PFOs treatment (Fig. 13). This suggests that, in the LTP experiments, also neurons can be damaged by 10 minutes of PFOs treatment, as well. However, neurons were still alive, since they were able to respond to the tetanic stimulation producing population spikes. As Angelova and Abramov showed, ROS production in primary neuronal culture is significantly higher after 8-10 minutes after oligomer exposure, compared to Monomer treatment[37]. We explain our LTP observations because of the Ca^{2+}-influx mechanism proposed before. In our hypothesis, once the Ca^{2+} ions flow into the cells through the amyloid pores, the unwanted depolarization induces an abnormal neurotransmitter release, synaptic

vesicle depletion, and unregulated postsynaptic Ca^{2+}-conductance, resulting in the impairment of synaptic transmission and synapse silencing[31]. This interpretation is supported by our preliminary results relative to mEPSC recordings (Fig. 25) and to the reduced levels of PSD-95 expression in brain slices used in the LTP experiments induced by sCT PFOs- but not by Monomer-enriched solutions, while presynaptic synaptophysin expression remained unchanged (Fig. 17).

Since the similarity in the effects described in the literature with other amyloid protein aggregates, a common amyloid-related excitotoxicity mechanism might exist, as proposed by Glabe[2]. We wonder how it could be possible to drive, so specifically, receptors or channels, using very different protein sequences? It is worth to note that, despite their sequence, all the amyloids appear to behave in the same common way.

Below we report the two FASTA sequences for sCT and $A\beta_{1-42}$ peptides, respectively 32 and 42 amino acids, obtained by UniProt[47], with the respective identifiers.

CSNLSTCVLGKLSQELHKLQTYPRTNTGSGTP
CALC1_ONCKE (P01263) [residues: 82 to 114]
AIVVGGVMLGIIAGKNSGVDEAFFVLKQHHVEYGSDHRFEAD
A4_HUMAN (P05067) [residues: 713 to 671]

Legend: Transmembrane APP, Hydrophobic, *polar*, **Charged**

These two sequences, without considering the transmembrane elements of $A\beta_{1-42}$, are similar in dimension (32 a.a. for sCT and 30 a.a. for $A\beta_{1-42}$) and show a core of about five highly hydrophobic residues enclosed within two segments of mixed hydrophobic and charged/polar modules located in similar positions, as well are very similar in the hydropathy profiles calculated using the Roseman hydrophobicity scale[48] (Fig.26).

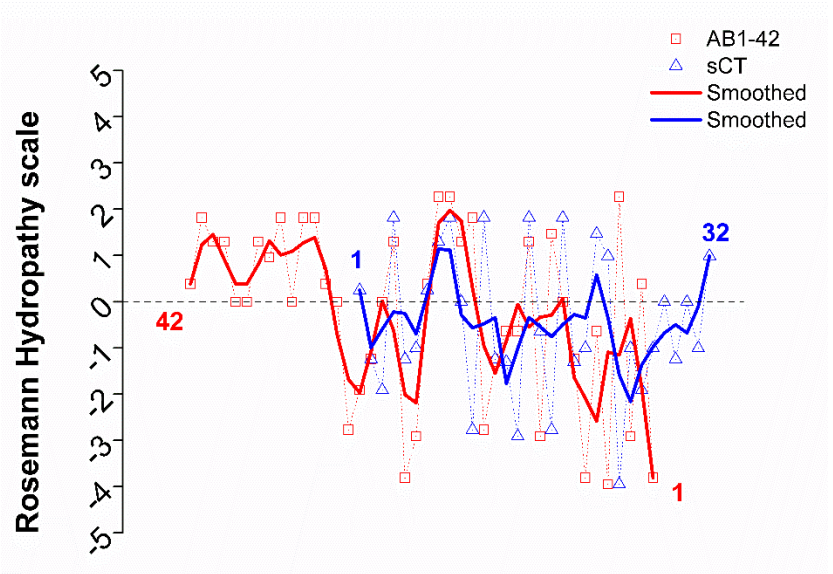

Figure 26- the hydropathy profile for sCT (blue) and Aβ$_{1-42}$ (red) residues, according to Roseman's scale[48]*. Increasing hydropathy values are reported as positive- while increasing hydrophilicity as negative-deflections. Notably, these profiles are very similar. Solid lines represent the smoothing trend by local averaging every three residues.*

We speculate that this common feature could be the structural basis from which similar PFOs are formed, characterized by a common hydrophobic/polar "outfit" and activating a common amyloid-mediated neurotoxicity mechanism. We stress this organization based on the idea that hydrophobic-hydrophilic profile, may influence the molecular dynamics of the interactions between PFOs and living membranes. This interaction takes place actually, as we demonstrated that aggregated sCT can interact with the charged head of GM1-ganglioside[29,42,49]. The research into the structure of this common "outfit" by biophysical techniques combined with molecular dynamics simulations would be very useful to elucidate this outstanding similarity. In other words, we speculate that this alternation between charged/polar and hydrophobic sequences might be pivotal to approach the membrane, and consequently, to induce toxicity.

According to the scenario depicted before, the data here reported here are in general agreement with the idea that the formation of amyloid pores could represent the initial phenomenon able to trigger the following NMDARs-mediated abnormal Ca^{2+}-influx, which leads to the neuronal impairment and damage. We named this process the "Amyloid mediated-excitotoxicity" paradigm (Fig. 27).

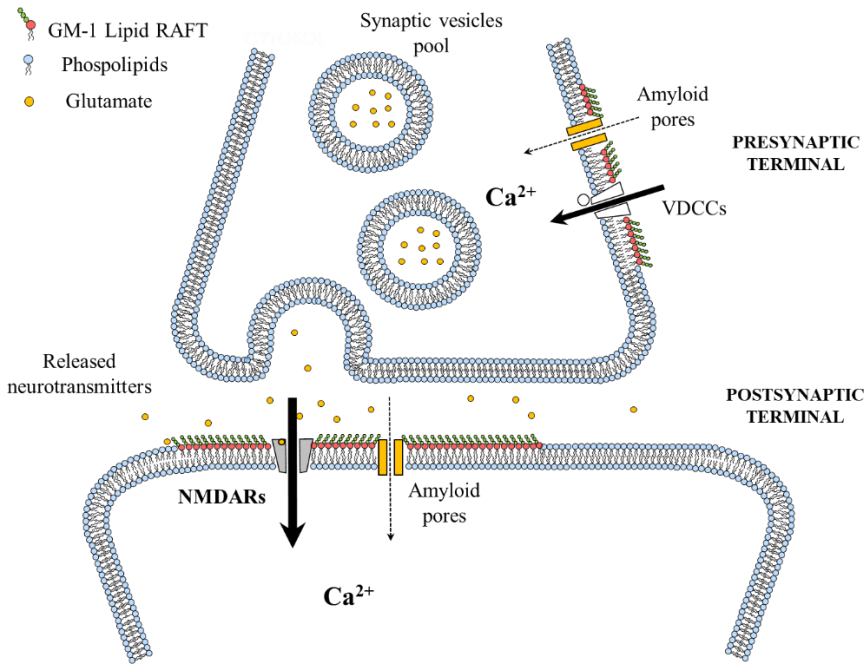

Figure 27 – "the amyloid mediated-excitotoxicity" paradigm. We suppose that early amyloid pore formation triggers an abnormal neurotransmitter release and thus an increased activation of N-Methil D-Aspartate Receptors (NMDARs) leading to intracellular calcium elevation, postsynaptic density disarrangement, impairment of synaptic strength and abrogation of Long Term Potentiation. Voltage-Dependent Calcium Channels (VDCCs)- and NMDARs-blockers/antagonists strongly revert this NMDARs- mediated toxicity[42].

In conclusion, our results could be important in the design of novel therapeutic approaches, which should follow three main routes: i) avoiding PFOs formation before they might interact with neuronal plasma membranes; ii) avoiding the binding between amyloid PFOs and GM1; iii) blocking amyloid pores once they were formed before the NMDA-mediated Ca^{2+}-influx is activated.

Material and methods

sCT samples preparation by Size Exclusion Chromatography (SEC). Monomer-enriched solutions at 1 mM sCT were prepared by dissolving sCT lyophilized powder (European Pharmacopoeia, EDQM, France) in desalted water. To limiting the aggregation process, the solution was rapidly frozen and stored at -80 °C. On the contrary, aggregated, native sCT solution was prepared by incubating 2 mg of sCT powder in 5 mM, phosphate buffer (PB: PB 5 mM, pH 7.4), at room temperature overnight. The aggregated and native solution was then loaded in the SEC column to purify oligomeric species enriched fractions3. Briefly, samples were loaded in the Sephadex G50-SEC column (GE HEALTHCARE, Milano, Italy- height: 500 mm, section: 20 mm). Column, maintained at 4 °C was pre-equilibrated at the same ionic strength of the samples and calibrated with a solution containing standards: BSA 1mg (66 kDa), Cytochrome C 1 mg (12.4 kDa-Combithek Boehringer, Mannheim, Germany), Aprotinin 1 mg (6.5 KDa) and Somatostatin 1mg (1.63 KDa) suspended in 5 mM PB buffer pH 7.4, and centrifuged at 15700 g × 10 min. Monomeric or aggregated sCT native solutions (0.5 mL aliquots), prepared as described above, were eluted in the column monitoring absorption at 280 nm by a variable wavelength UV detector (BIORAD Econo UV monitor, Hercules, CA). Fractions collected (Gilson FC 203B, 1.4 mL/fraction) were administered directly in cell cultures, to test their effects on cellular viability and calcium imaging and in hippocampus slices to evaluate LTP. The final concentrations of sCT fractions used in these experiments were 8 μM.

Photo-induced Cross-linking of Unmodified Proteins (PICUP) and tricine SDS-PAGE Gel characterization. Aiming to obtain an electrophoretic characterization (tricine/SDS-PAGE) of the fraction eluted, samples were stabilized to prevent oligomers misfolding in a reducing environment. We, therefore, treated them for PICUP. The original protocol was adapted by Diociauti et al.[43]. Briefly, for each sample, we prepared a 20 μl volume containing 80 μM Oligomers, 50 μM Tris (2,2 bipyridyl) dichlororuthenium (II) hexahydrate) and 1mM ammonium persulfate (SIGMA). Cross-linking reaction occurred irradiating samples for 2 s with a 100 W white lamp in a dark room, the

reaction was quickly quenched adding 20 µl of reducing sample buffer containing 5 % β-MeOH and boiled for 5 minutes. Samples were finally analyzed by tricine/SDS-PAGE. Separating gel: 10% Acrylamide/Bis (32:1) (ICN Biomedicals, Inc., Aurora, Ohio USA/Fluka, Buchs, CH); spacer gel 6.5 % Acrylamide/Bis and stacking gel: 2.5 % Acrylamide/Bis. For each lane were run 40 µl of the sample buffer, or 8 µl of molecular weight markers (Color Marker Ultralow Range - SIGMA, cat n° C6210-1VL). Then gels were stained by the silver procedure. Finally, gel band densitometry has been performed using the imaging freeware ImageJ. For each lane, a grey-scale optical density profile has been obtained, including molecular weight markers (1.3 KDa, 3.5 KDa, 6.5 KDa, 14.4 KDa, 17.,0 KDa, 26.6 KDa). Peaks corresponding to sCT prefibrillar oligomers: Monomers, dimers, trimers-tetramers, pentamers, and octamers have been individuated according to the molecular weight marker profile. Gel densitometry was used to compute two estimators, named PFOs % index and Average MW index, considering the oligomers species that prevalently populated the fractions. The values were used to evaluate statistical differences between sCT monomeric and aggregated samples.

Energy Filtered-Transmission Electron Microscopy (EF-TEM). We used a Transmission Electron Microscope model TECNAI 12 G2 Twin (FEI Company, Hillsboro, OR, USA) equipped with a thermionic gun (single-crystal lanthanum hexaboride) and energy dispersive X-ray spectrometer (model Genesis 4000, EDAX Inc., Mahwah, NY, USA) and post-column electron energy filter (Biofilter, GATAN Inc., Pleasanton, CA, USA). The energy-filtered images were acquired by a slow-scan CCD camera (model 794 IF, GATAN Inc., Pleasanton, CA, USA). Conventional imaging was performed in energy-filtered image mode configuration at an electron energy of 120 keV, with a collection angle of about 20 mrad. To enhance image contrast and resolution, chromatic aberrations were reduced by collecting only elastic electrons (ΔE=0)61.

Cell cultures. HT22 cells were developed from their analogous HT4 cells, immortalized from primary mouse hippocampal neurons. If grown without establishing synaptic connections, both HT22 and HT4

hippocampal cells can develop LTP, in terms of neurotransmitter release29. HT22 neuronal cell line in proliferating conditions doesn't express cholinergic and glutamatergic receptors, although HT22 cells can also be differentiated in a selective medium, changing their morphology and inducing expression of cholinergic markers like choline acetyltransferase (ChAT), vesicular acetylcholine transporter (VAChT), high-affinity choline transporter (HACT), muscarinic M1 and M2 subunit of Ach- receptors. Moreover, they become susceptible to glutamate excitotoxicity52,62 _ENREF_3 that is mainly mediated by NMDARs63 via Ca2+-influx64, but also by several second messengers like nitric oxide65, calpain-1/poly-(ADP-ribose) polymerase1/apoptosis inducing factor66, free radicals and mitochondria67. NMDAR antagonists, such as Dizocilpine (MK801), can effectively prevent glutamate-induced excitotoxicity52.

HT22 cells were maintained at 37 °C, 10%, CO2 in Dulbecco's modified Eagle's medium (DMEM, Sigma Aldrich–D6546) supplemented with 10% heat-inactivated FBS and kept at less than 50% of confluence. Differentiation was carried out in the Neurobasal medium (NBM, Gibco, 21103-49) containing N2 supplement (Gibco-17502048), at least for 24-48 hours before use.

Primary hippocampal co-cultures (neurons and glia) have been prepared from postnatal day 2-mouse brain. All experimental procedures were carried out according to the Italian law and to "Ethical guidelines for scientific experimentation on animals". The experimental protocol was approved by the Italian Ministry of Public Health (authorization n. 86/2018-PR) and was following guidelines of the European Union Council Directive (86/609/European Economic Community). After dissection, hippocampi were incubated 15 minutes at 37 °C, with 0.25 % trypsin (Gibco, 15090-046) and then dissociated in NeuroBasal medium (Gibco, 21103-49) containing 10% heat-inactivated FBS, 50 µg/mL gentamicin (Gibco, 15750-037), 1x Glutamax (Gibco, 35050-038). Cells were seeded on 48-wells plates for MTT assay or on sterile glass coverslips (diameter 12 mm), previously coated with 1x poly-L-lysine (Sigma-Aldrich), in 24-wells plates, for Fura2-AM experiments or GM1 evaluation. After plating cell cultures were rapidly stored in the cell incubator (5% CO2, 37 °C). After 2 hours, the cell culture medium was replaced with 700 µl/well of

Neurobasal medium containing 1X B27 supplement (Gibco, 17504-044) instead of FBS. Hippocampal co-cultures were used at 6 DIV (not fully mature culture) or 14 DIV (fully mature culture).

Fura2-AM Ca^{2+} imaging recordings in cell cultures. For evaluation of the intracellular Ca2+ ([Ca2+]i), 1 mM Fura-2 Acetoxy Methyl ester (Fura-2 AM, Thermo Fisher Scientific - F1221) stock solution was prepared dissolving Fura2-AM lyophilized salt in 75% DMSO, 25% pluronic acid (Thermo Fisher Scientific, F-127), sonicated for 5 minutes in darkness, at RT. 5 μM Fura-2AM solution was diluted from stock solution in fresh Ringer extracellular solution (NaCl 125 mM, KCl 1 mM, $MgCl_2$ 1.5 mM, $CaCl_2$ 2 mM, HEPES 20 mM, D-Glucose 8 mM, 300 mOsm, pH 7.4 with NaOH). Cell-seeded coverslips were incubated with Fura-2AM working solution for 50 minutes at 37 °C, 5% CO2 in darkness. After three washes in the Ringer solution, coverslips were rapidly placed in the cell bath with fresh Ringer solution on the microscope stage, for Ca2+ imaging recordings. All recordings were performed in dark conditions. After 2 minutes of adaptation (baseline), samples from different native sCT fractions were used to treat the cells, at a final concentration of 8 μM. fluorimetric recordings with Fura-2AM were performed along the experiment to obtain ratiometric measurements of the [Ca2+]i that is the ratio between the emission intensities measured at 510 nm, stimulated at 340 nm and 380 nm68. One acquisition was done each 6 seconds, along 15 minutes, on a region of interest in the cellular bodies. Ratios and 340 nm and 380 nm background signals, from time-lapse sequence images, were obtained by the imaging freeware ImageJ. Data were plotted by the software: Microcal Origin 8.

MTT and TUNEL assay in cell cultures. Cell viability was evaluated by the 3-(4,5-dimethylthiazol-2-yl)-2,5-diphenyltetrazolium bromide (MTT) assay; the MTT assay has been widely used to assess cell viability and is based on the ability of viable cells to reduce MTT, giving rise to an insoluble purple formazan salt. Briefly, the cultures were incubated for 20 minutes at 37 °C with 0.5 mg/ml MTT in Hank‘s balanced salt solution (Life Technologies). The reaction product was dissolved in dimethyl sulphoxide. The spectral photometric absorbance

of the samples was determined at a wavelength of 540 nm. The amount of MTT conversion was evaluated as a percentage of the absorbance measured in treated cells relative to the absorbance of control cells. After fixation in 4% paraformaldehyde in PBS, 0.12 M in sucrose, apoptosis was evaluated in mixed hippocampal cultures by the terminal transferase-mediated dUTP-biotin nick end-labelling (TUNEL) assay (DeadEnd kit, Promega, Madison, WI).

Long Term Potentiation (LTP) in mouse hippocampal slices. Wild type BALB/c mice aged 6 to 9 weeks were used following guidelines and regulations of the European Union Council Directive (86/609/European Economic Community). All the experimental protocols were approved by the Italian Ministry of Public Health (authorization n. 86/2018-PR). Under anaesthesia with halothane (2-Brom-2-Chlor-1,1,1-trifluoro-Ethan), the animals were decapitated, and brains were quickly removed and placed in the cold, oxygenated artificial cerebral spinal fluid (ACSF), whose composition in mM was: NaCl 124, KCl 2, KH_2PO_4 1.25, $MgSO_4$ 2, $CaCl_2$ 2, $NaHCO_3$ 26, and Glucose 10. The hippocampal slices were prepared according to conventional procedures[50]. The hippocampus was rapidly dissected and slices (450 µm thick) were cut transversely by a chopper (McIlwain Tissue Chopper) and transferred into an interface tissue chamber constantly perfused by a flow of 1.2 mL/min of ACSF and humidified gas (95% O2 – 5% CO2) at 32-34 °C (pH 7.4). According to the original protocol70, extracellular recordings of the population spikes (PSs) were made in the *stratum pyramidale* of the CA1 subfield using glass microelectrodes filled with 2 M NaCl (resistance 5-10 MΩ). Orthodromic stimuli (10-500 mA, 20-90 ms, 0,1 Hz) were delivered through a platinum electrode placed in the Schaffer collateral commissural pathways in the *stratum radiatum*. The test stimulus intensity of 50 ms square pulses was adjusted to elicit a PS of 2-3 mV at 0,03 Hz. Each minute, a trace was calculated as the average of six recordings every 10 seconds. After recording stable signals (20-30 minutes), the hippocampal slices were treated with Monomer- or PFOs-enriched solutions of sCT, to assay their effects on synaptic plasticity. PFOs and Monomers were diluted in carboxygenate ACSF at a final concentration of about 2 µM: the slices were then superfused.

After 20 minutes from the administration of sCT, a tetanic stimulation (100 Hz, 1 s) was delivered to induce LTP at the same stimulus intensity used for the baseline responses. Field potentials were fed to a computer interface (Digidata 1440A, Axon Instruments, Foster City, CA) for subsequent analysis with the software PCLAMP10 (Axon Instruments).

Western blot (WB) analysis. Hippocampal 450 μm-thick transversely coronal slices were homogenized in extraction buffer (25 mM Tris–HCl, pH 7.4, 150 mM NaCl, 1% Triton X-100, 0.1% SDS, 1% sodium deoxycholate, 1 mM sodium orthovanadate, 1 mM sodium fluoride, 1 mM PMSF, and a protease inhibitor cocktail) on ice for 30 minutes and centrifuged at 100.000 × g for 1 h, at 4 °C. The protein concentration was determined using the Micro BCA Protein Assay Kit (Pierce, Rockford, IL, USA). Proteins (30 μg) were separated on 12% SDS-PAGE and transferred to nitrocellulose membranes at 35 V overnight. The membranes were blocked at room temperature in 3% BSA and incubated overnight at 4 °C with the following primary antibodies: mouse monoclonal anti-PSD-95, rabbit polyclonal anti-synaptophysin (home-made) and, as a control for protein loading, mouse monoclonal anti-β-actin (Santa Cruz). The membranes were washed and incubated with the appropriate peroxidase-labelled secondary antibody (Bio-Rad, Hercules, CA, USA) for 1 h at room temperature. After extensive washes in TTBS (20 mM Tris–HCl, pH 7.4, 0.15 M NaCl, 0.1 % Tween 20), the immunoreactive bands were detected by enhanced chemiluminescence coupled to peroxidase activity (Santa Cruz Biotech) and imaged with a ChemiDoc XRS system (Bio-Rad Laboratories Inc.).

Immunofluorescence. Hippocampal 450 μm-thick transversely coronal slices were treated or not with sCT PFOs- or Monomer-enriched solutions for 100 min. After treatment, the slices were fixed overnight with 4% paraformaldehyde in PBS, 0.12 M in sucrose. After fixation, the samples were rinsed three times in PBS with 5% sucrose and 0.15 mM CaCl2 and left overnight in sucrose buffer (PBS with 30% sucrose and 0.15 mM CaCl2). Samples were then embedded in Tissue Freezing Medium (Jung, Germany), frozen at -30 °C in isopentane and stored at -80°C. Sections (8 μm) were cut at a Leica CM 1860 UV

cryostat and labelled with primary antibodies overnight at 4°C. The following primary antibodies were used: monoclonal anti-NeuN (Millipore, USA) rabbit anti-PSD-95 (Cell Signaling Technology, Danvers, MA) and monoclonal anti-synaptophysin (BD Transduction Laboratories, Franklin Lakes, NJ). Primary antibodies were revealed with secondary antibodies coupled to Alexa Fluor® 488 and Alexa Fluor® 546 (Invitrogen), diluted 1:250 PBS (45 min, 37 °C). Sections were counterstained with Hoechst 33258; the dye, which binds specifically to A–T base regions in DNA and emits blue immunofluorescence at 350 nm, was administered at 1 ng/ml for 1 minute. Sections were observed at an Eclipse 80i Nikon Fluorescence Microscope (Nikon Instruments, Amsterdam, The Netherlands), equipped with a Video Confocal (ViCo) system.

GM1 expression. To analyze GM1 localization in HT22 cells and hippocampal neurons we used Alexa Fluor 488–conjugated cholera toxin-β (CT β, Molecular Probes, Eugene, OR) (10 μg/mL). After fixation in 4% paraformaldehyde in PBS, 0.12 M in sucrose, cultures were stained with CTβ at room temperature for 30 minutes. To highlight nuclei, cultures were counterstained with Hoechst 33258. Cultures were observed at an Eclipse 80i Nikon Fluorescence Microscope (Nikon Instruments, Amsterdam, The Netherlands), equipped with a Video Confocal (ViCo) system.

inside-out Excised Patch Clamp recordings

The experimental procedure was made according to Bode and colleagues46. In turn: patch pipette was obtained from borosilicate thin-wall capillary (World Precision Instruments Patch pipette (typically Rpip 7MΩ) were made by a vertical puller (Narishige).

Patch-clamp recordings were performed on the excised patch of membrane from mice primary hippocampal neurons at 14 DIV, in voltage-clamp mode. Recordings were realized in extracellular solutions whose composition in mM was: 121.4 NaCl, 2.16 KCl, 10 CsCl, 10 HEPES, 1.87 $CaCl_2$, 1.87 $MgCl_2$, 0.1 EGTA. Osmolarity was adjusted to 300 mOsm with sucrose and pH to 7,4. To block endogenous conductances, specific drug blockers/antagonists were

added in the solution: 1µM TTX, 10mM TEA, 100µM APV, 10µM CNQX, 100µM Bicuculline.
To better gain the giga-ohm sealing, about one millimetre of the pipette tip was filled with symmetrical solution then patch pipette was backfilled with the same solution containing samples (sCT-Monomers and -PFOs) at a final concentration of 8µM. As a positive control for membrane permeabilization, we used Amphotericin B a very well-known ionophore (the concentration recommended in the datasheet was 150 µg/mL). Once the giga-Ohm seal was obtained, the pipette was gently retracted until a reduction in the capacitive transients, assessing the formation of a small vesicle on the pipette tip. Then the pipette tip was gently retracted outside the bath. Once the pipette tip was exposed to the air, the outer portion of the vesicle rapidly broke-up. Then the pipette was soaked again in the bath, exposing its intracellular side toward the external solution. Another deep reduction in the transients stating that the inside-out mode was achieved. The holding potential was set to 0 mV. Patch of membranes were stimulated with a series of voltage potentials whose amplitude in mV was:0, +60, +40, +20, 0, -20, -40, -60, 0 (step duration was 250 ms) utilizing an Axopatch 200A amplifier (Axon Instrument, Union City, CA) supported with PClamp10 software. Recordings were sampled at a rate of 2KHz with a for poles-low pass Bessel filter frequency of 1KHz. Transmembrane currents were recorded for about 40 minutes. Quality controls were: $R_{seal} > 1$ GΩ; $R_{series} < 20$ MΩ.

spontaneous mEPSC recordings.

Mice Hippocampal neurons at 14DIV were superfused with extracellular solutions whose composition in mM was: 120 NaCl, 4.2 KCl, 10 HEPES, 2 $CaCl_2$, 0,3 $MgCl_2$, 10 Glucose. Osmolarity was adjusted to 300 mOsm with sucrose and pH to 7,4. The intracellular solution composition in mM was: 125 K-Gluconate, 2 $CaCl_2$, 2 $MgCl_2$, 10 EGTA, 10 HEPES, 2 Na_2-ATP, 0.5 Na_2-GTP. 4-5 MΩ Patch electrodes were typically used in these experiments. Once the giga-Ohm seal was achieved the patch was broken by a pulse of suction going in the whole-cell mode. Cells were clamped at the holding potential of-65mV, and spontaneous current sweeps of 0.5 seconds were recorded one each a minute, for about 10 minutes

During recordings, a potential of 1mV was applied to measure the stability of the seal resistance, every 2 seconds. Traces were accounted for in the analysis only within a fluctuation in 5% on the mean value and less than 1mV in drift. To measure spontaneous miniature EPSC, 1µM TTX, 100µM APV, and 100µM Bicuculline were added in the extracellular- and in intracellular-solution, to block Na+ channels GABA-A channels and NMDARs, leaving AMPARs permissive.
mEPSC was recorded using the Axopatch 200A amplifier (Axon Instrument, Union City, CA) supported with PClamp10 software. Recordings were sampled at a rate of 2KHz with a for poles-low pass Bessel filter frequency of 1KHz.

Statistical analysis

Average Molecular Weight and PFOs % indexes. We computed two estimators from gel densitometry, named:

$$Average\ MW\ index\ (AMWi-\ kDa) = \sum_{i=1}^{n} Ai \cdot mw_i$$

(A_i: Area under the i-meric species band peak)
and

$$PFOs\ \%\ index = \left(\frac{1}{A_t} \cdot \sum_{i=1}^{n} A_{Te+Tr+P+H}\right) \cdot 100$$

($A_{Te+Tr+P+H}$: Area under the trimeric, tetrameric, pentameric and hexameric species band peaks, Ai: total area under the gel densitometry lane).

These indexes were plotted as a boxplot. A non-parametric test was computed to assess the statistical significance of indexes differences, for Monomer- and PFOs-enriched samples, with a confidence level of 95%, under the null hypothesis H_0: AMWi $_{Monomers}$ = AMWi $_{samples}$ or PFOs% $_{Monomers}$ = PFOs% $_{samples}$.

Intracellular Ca^{2+}. Peaks and end-time values of the $[Ca2^+]_i$, were calculated over the experiments and expressed as a percentage of the Baseline-Corrected-Ratio values. Statistical significance of the $[Ca2^+]_i$ differences, between Monomers vs PFOs, treated neurons was assessed under the null hypothesis: H0a ($[Ca2^+]_i$) Monomers = ($[Ca2^+]_i$) PFO, utilizing T-test, with a confidence level of 95% and 99%. A multiple comparison in the effects of PFOs administration upon drugs pre-treatments with MK801 and Verapamil or in the effects of PFOs administration on cells in different maturating conditions (undifferentiated HT22, differentiated HT22, HpC neurons 6 DIV, and HpC neurons 14 DIV), was assessed respectively through one-way ANOVA, followed by Dunnett post-tests or for multiple comparison by Bonferroni correction.

MTT. Cellular viability estimations for each experimental condition were obtained in quadruplicate, from the MTT assay. Data were normalized respect to controls. Multiple comparisons in cellular viability were obtained concerning controls for all experimental conditions, utilizing ANOVA followed by Dunnett test, with a confidence level of 95 % and 99%.

LTP. The maximal slopes of the descending and ascending branches of the PS were averaged in the module and plotted against the corresponding experimental time. For each trace, raw data were normalized as a percentage of the baseline PS slope, before test substances administration. Statistical significance in differences for all experimental conditions was assessed by means of an ANOVA followed by Bonferroni correction, respect to the basal transmission and the end-time values, (80 minutes after the tetanic stimulation), with a confidence of 95% and 99%.

References

1. Bitan, G. & Teplow, D. B. Rapid photochemical cross-linking--a new tool for studies of metastable, amyloidogenic protein assemblies. *Acc Chem Res* **37**, 357–364 (2004).
2. Dobson, C. M. Principles of protein folding, misfolding and aggregation. *Semin. Cell Dev. Biol.* **15**, 3–16 (2004).
3. Dobson, C. M. Protein folding and misfolding. *Nature* **426**, 884–90 (2003).
4. Ponomarenko, E. A. *et al.* The Size of the Human Proteome: The Width and Depth. *Int. J. Anal. Chem.* **2016**, (2016).
5. Dobson, C. M., Šali, A. & Karplus, M. Protein Folding: A Perspective from Theory and Experiment. *Angew. Chemie Int. Ed.* **37**, 868–893 (1998).
6. Dinner, A. R., Sali, A., Smith, L. J., Dobson, C. M. & Karplus, M. Understanding protein folding via free-energy surfaces from theory and experiment. *Trends Biochem. Sci.* **25**, 331–9 (2000).
7. Mogk, A., Bukau, B. & Kampinga, H. H. Cellular Handling of Protein Aggregates by Disaggregation Machines. *Mol. Cell* **69**, 214–226 (2018).
8. Schnabel, J. Protein folding: The dark side of proteins. *Nature* **464**, 828–9 (2010).
9. Vendruscolo, M., Zurdo, J., MacPhee, C. E. & Dobson, C. M. Protein folding and misfolding: a paradigm of self-assembly and regulation in complex biological systems. *Philos. Trans. A. Math. Phys. Eng. Sci.* **361**, 1205–22 (2003).
10. Bukau, B. & Horwich, A. L. The Hsp70 and Hsp60 chaperone machines. *Cell* **92**, 351–66 (1998).
11. Schiene, C. & Fischer, G. Enzymes that catalyzese the restructuring of proteins. *Curr. Opin. Struct. Biol.* **10**, 40–5 (2000).
12. Xu, C. & Ng, D. T. W. Glycosylation-directed quality control of protein folding. *Nat. Rev. Mol. Cell Biol.* **16**, 742–752 (2015).
13. Bence, N. F., Sampat, R. M. & Kopito, R. R. Impairment of the ubiquitin-proteasome system by protein aggregation. *Science* **292**, 1552–5 (2001).
14. Dobson, C. M. Protein misfolding, evolution and disease. *Trends Biochem. Sci.* **24**, 329–32 (1999).
15. Valastyan, J. S. & Lindquist, S. Mechanisms of protein-folding

diseases at a glance. *Dis. Model. Mech.* **7**, 9–14 (2014).
16. Stefani, M. & Dobson, C. M. Protein aggregation and aggregate toxicity: new insights into protein folding, misfolding diseases and biological evolution. *J. Mol. Med. (Berl).* **81**, 678–99 (2003).
17. Dobson, C. M. The structural basis of protein folding and its links with human disease. *Philos. Trans. R. Soc. London. Ser. B Biol. Sci.* **356**, 133–145 (2001).
18. Balbirnie, M., Grothe, R. & Eisenberg, D. S. An amyloid-forming peptide from the yeast prion Sup35 reveals a dehydrated -sheet structure for amyloid. *Proc. Natl. Acad. Sci.* **98**, 2375–2380 (2001).
19. Aguzzi, A. Beyond the prion principle. *Nature* **459**, 924–925 (2009).
20. Clark, M. S. *et al.* Calcitonin: characterisation and expression in a teleost fish, Fugu rubripes. *J. Mol. Endocrinol.* **28**, 111–23 (2002).
21. Malchiodi-Albedi, F., Vanacore, N. & Diociaiuti, M. Calcitonin therapy and oligomer neurotoxicity: An underestimated risk? *Neurotoxicology* **29**, 1150–1151 (2008).
22. Arvinte, T., Cudd, A. & Drake, A. F. The structure and mechanism of formation of human calcitonin fibrils. *J Biol Chem* **268**, 6415–6422 (1993).
23. Kamgar-Parsi, K. *et al.* Structural Biology of Calcitonin: From Aqueous Therapeutic Properties to Amyloid Aggregation. *Isr. J. Chem.* **57**, 634–650 (2017).
24. Benilova, I., Karran, E. & De Strooper, B. The toxic Aβ oligomer and Alzheimer's disease: an emperor in need of clothes. *Nat. Neurosci.* **15**, 349–57 (2012).
25. Allen, J. A., Halverson-Tamboli, R. A. & Rasenick, M. M. Lipid raft microdomains and neurotransmitter signalling. *Nat Rev Neurosci* **8**, 128–140 (2007).
26. Abramov, A. Y., Canevari, L. & Duchen, M. R. Calcium signals induced by amyloid beta peptide and their consequences in neurons and astrocytes in culture. *Biochim Biophys Acta* **1742**, 81–87 (2004).
27. Volles, M. J. *et al.* Vesicle Permeabilization by Protofibrillar α-Synuclein: Implications for the Pathogenesis and Treatment of Parkinson's Disease †. *Biochemistry* **40**, 7812–7819 (2001).
28. Quist, A. *et al.* Amyloid ion channels: A common structural

link for protein-misfolding disease. *Proc. Natl. Acad. Sci.* **102**, 10427–10432 (2005).
29. Diociaiuti, M. *et al.* Monosialoganglioside-GM1 triggers binding of the amyloid-protein salmon calcitonin to a Langmuir membrane model mimicking the occurrence of lipid-rafts. *Biochem Biophys Rep* **8**, 365–375 (2016).
30. Sokolov, Y. *et al.* Soluble Amyloid Oligomers Increase Bilayer Conductance by Altering Dielectric Structure. *J. Gen. Physiol.* **128**, 637–647 (2006).
31. Kayed, R. *et al.* Permeabilization of Lipid Bilayers Is a Common Conformation-dependent Activity of Soluble Amyloid Oligomers in Protein Misfolding Diseases. *J. Biol. Chem.* **279**, 46363–46366 (2004).
32. Shafrir, Y., Durell, S., Arispe, N. & Guy, H. R. Models of membrane-bound Alzheimer's Abeta peptide assemblies. *Proteins Struct. Funct. Bioinforma.* **78**, 3473–3487 (2010).
33. Bode, D. C., Baker, M. D. & Viles, J. H. Ion Channel Formation by Amyloid-β_{42} Oligomers but Not Amyloid-β_{40} in Cellular Membranes. *J. Biol. Chem.* **292**, 1404–1413 (2017).
34. Luscher, C. & Malenka, R. C. NMDA receptor-dependent long-term potentiation and long-term depression (LTP/LTD). *Cold Spring Harb Perspect Biol* **4**, (2012).
35. Texidó, L., Martín-Satué, M., Alberdi, E., Solsona, C. & Matute, C. Amyloid β peptide oligomers directly activate NMDA receptors. *Cell Calcium* **49**, 184–190 (2011).
36. Peters, C., Sepulveda, F. J., Fernandez-Perez, E. J., Peoples, R. W. & Aguayo, L. G. The Level of NMDA Receptor in the Membrane Modulates Amyloid-beta Association and Perforation. *J Alzheimers Dis* **53**, 197–207 (2016).
37. Renner, M. *et al.* Deleterious effects of amyloid beta oligomers acting as an extracellular scaffold for mGluR5. *Neuron* **66**, 739–754 (2010).
38. Kim, M. J. *et al.* Synaptic accumulation of PSD-95 and synaptic function regulated by phosphorylation of serine-295 of PSD-95. *Neuron* **56**, 488–502 (2007).
39. Wang, Q., Walsh, D. M., Rowan, M. J., Selkoe, D. J. & Anwyl, R. Block of long-term potentiation by naturally secreted and synthetic amyloid beta-peptide in hippocampal slices is mediated via activation of the kinases c-Jun N-terminal kinase, cyclin-dependent kinase 5, and p38 mitogen-

activated protein kinase as well a. *J Neurosci* **24**, 3370–3378 (2004).
40. He, M., Liu, J., Cheng, S., Xing, Y. & Suo, W. Z. Differentiation renders susceptibility to excitotoxicity in HT22 neurons. *Neural Regen Res* **8**, 1297–1306 (2013).
41. Li, S. *et al.* Soluble Abeta oligomers inhibit long-term potentiation through a mechanism involving excessive activation of extrasynaptic NR2B-containing NMDA receptors. *J Neurosci* **31**, 6627–6638 (2011).
42. Belfiore, M. *et al.* Calcitonin native prefibrillar oligomers but not monomers induce membrane damage that triggers NMDA-mediated Ca2+-influx, LTP impairment and neurotoxicity. *Sci. Rep.* **9**, 5144 (2019).
43. Diociaiuti, M. *et al.* Native metastable prefibrillar oligomers are the most neurotoxic species among amyloid aggregates. *Biochim. Biophys. Acta - Mol. Basis Dis.* **1842**, 1622–1629 (2014).
44. Kamgar-Parsi, K. *et al.* Structural Biology of Calcitonin: From Aqueous Therapeutic Properties to Amyloid Aggregation. *Isr. J. Chem.* **57**, 634–650 (2017).
45. Lecture, N. & Neher, E. *ION CHANNELS FOR COMMUNICATION BETWEEN AND WITHIN CELLS*. (1991).
46. Belfiore, M. *et al.* Calcitonin native prefibrillar oligomers but not monomers induce membrane damage that triggers NMDA-mediated Ca2+-influx, LTP impairment and neurotoxicity. *Sci. Rep.* **9**, 5144 (2019).
47. Align. Available at: https://www.uniprot.org/align/. (Accessed: 21st July 2019)
48. Roseman, M. A. Hydrophilicity of polar amino acid side-chains is markedly reduced by flanking peptide bonds. *J. Mol. Biol.* **200**, 513–522 (1988).
49. Malchiodi-Albedi, F. *et al.* Lipid raft disruption protects mature neurons against amyloid oligomer toxicity. *Biochim Biophys Acta* **1802**, 406–415 (2010).
50. D'Arcangelo, G. *et al.* Glutamatergic neurotransmission in a mouse model of Niemann-Pick type C disease. *Brain Res* **1396**, 11–19 (2011).

Ringraziamenti

"*...Non c'è nessun lavoro che, allo stesso tempo, metta insieme: fantasia, creatività e sapere come la Ricerca." Questa* la riflessione di un mio vecchio capo, in un giorno cupo di febbraio di qualche tempo orsono, quando ancora non avevo messo bene a fuoco che cosa volessi fare nella vita; una frase che nella sua semplicità mi ha spiazzato e che con il tempo ha creato in me una rivoluzione. Molti anni sono passati da quel giorno e devo dire che alla fine ho fatto mia questa suggestione.

Da ragazzo sono sempre stato curioso e affascinato dalla natura e dal sapere, spesso ho pensato che un giorno sarei potuto diventare un uomo di scienza… la parola "Ricerca" mi ha sempre portato alla mente i versetti de" La Divina Commedia" *(Inferno, canto XXVI):*
[*... Considerate la vostra semenza:* f*atti non foste a viver come bruti, ma per seguir virtute e canoscenza*] *(vv. 118-120).*

Questa la frase che il sommo poeta, mette in bocca ad Ulisse per accendere l'animo dei suoi uomini ed indurli a travalicare i limiti di ciò che quelli ritenevano impossibile, a gettare il cuore oltre l'ostacolo a qualunque costo; una frase che ben si adatta a chi fa il lavoro di Ricercatore in Italia: un lavoro duro, precario e sottopagato.

Dante tuttavia, ci ammonisce di non perseguire l'obiettivo della conoscenza con superbia, traditi cioè dal proprio ego e ammaliati esclusivamente dall'apparenza, per evitare di essere sopraffatti da ciò che si cela ma che è sostanziale, …come fece l'astuto Odisseo che per questo è dannato.
[... Li miei compagni fec'io sì aguti, con questa orazion picciola, al cammino, che a pena poscia li avrei ritenuti e volta nostra poppa nel mattino, de' remi facemmo ali al folle volo, sempre acquistando dal lato mancino.] (vv. 121-126) [...quando n'apparve una montagna, bruna per la distanza, e parvemi alta tanto quanto veduta non avëa alcuna. Noi ci allegrammo, e tosto tornò in pianto, ché de la nova terra un turbo nacque, e percosse del legno il primo canto. Tre volte il fé girar con tutte l'acque; a la quarta levar la poppa in suso e la prora ire in giù, com'altrui piacque infin che 'l mar fu sovra noi richiuso.] (vv. 133-142).

Se qualcosa il dottorato mi ha insegnato è che l'unica via che porta alla

vera conoscenza si chiama umiltà!

Questo lungo percorso che mi ha permesso infine di ottenere il titolo di Dottore di Ricerca è stato una lenta e sofferta metamorfosi, verso un modo di pensare e di ragionare nuovo e irreversibile, molti sono stati i momenti oscuri in cui mi sono più volte perso e ritrovato, pochi ed intensi quelli belli ed indimenticabili.
Alla fine del viaggio, tante le cicatrici profonde, ma grande anche la soddisfazione di essere stato determinato.

È giusto tuttavia, constatare che se qualcosa di positivo ho compiuto, il merito di ciò risiede prima di tutto nell'appoggio incondizionato e nel sostegno materiale e spirituale di coloro che hanno condiviso con me questo percorso: in primo luogo della mia famiglia in particolare di mia Moglie Simona e di mio figlio Michele che mi hanno sempre sostenuto con il loro Amore, dei miei genitori che mi hanno aiutato a superare le non poche difficoltà di questi anni e mi hanno spinto a cercare in me la forza di perseguire gli obiettivi che mi ero posto.

Ringrazio i miei mentori e colleghi che hanno reso possibile il concretizzarsi di questo lavoro di Ricerca in particolare il Dr Marco Diociaiuti e il Dr Claudio Frank.

Ringrazio infine la Prof.ssa Maria Egle De Stefano per tutto il supporto fornitomi.